www.nature.com/aps

Acta Pharmacologica Sinica

ARTICLE

SZC-6, a small-molecule activator of SIRT3, attenuates cardiac hypertrophy in mice

Ze-yu Li[1], Guo-qing Lu[2], Jing Lu[1], Pan-xia Wang[1], Xiao-lei Zhang[2], Yong Zou[2] and Pei-qing Liu[1]

Sirtuin3 (SIRT3), a class III histone deacetylase, is implicated in various cardiovascular diseases as a novel therapeutic target. SIRT3 has been proven to be cardioprotective in a model of Ang II-induced cardiac hypertrophy. However, a few small-molecule compounds targeting deacetylases could activate SIRT3. In this study, we generated a novel SIRT3 activator, 3-(2-bromo-4-hydroxyphenyl)-7-hydroxy-2H-chromen-2-one (SZC-6), through structural optimization of the first SIRT3 agonist C12. We demonstrated that SZC-6 directly bound to SIRT3 with K_d value of 15 μM, and increased SIRT3 deacetylation activity with EC_{50} value of 23.2 ± 3.3 μM. In neonatal rat cardiomyocytes (NRCMs), pretreatment with SZC-6 (10, 20, 40 μM) dose-dependently attenuated isoproterenol (ISO)-induced hypertrophic responses. Administration of SZC-6 (20, 40 and 60 $mg{\cdot}kg^{-1}{\cdot}d^{-1}$, s.c.) for 2 weeks starting from one week prior ISO treatment dose-dependently reversed ISO-induced impairment of diastolic and systolic cardiac function in wild-type mice, but not in SIRT3 knockdown mice. We showed that SZC-6 (10, 20, 40 μM) dose-dependently inhibited cardiac fibroblast proliferation and differentiation into myofibroblasts, which was abolished in SIRT3-knockdown mice. We further revealed that activation of SIRT3 by SZC-6 increased ATP production and rate of mitochondrial oxygen consumption, and reduced ROS, improving mitochondrial function in ISO-treated NRCMs. We also found that SZC-6 dose-dependently enhanced LKB1 phosphorylation, thereby promoting AMPK activation to inhibit Drp1-dependent mitochondrial fragmentation. Taken together, these results demonstrate that SZC-6 is a novel SIRT3 agonist with potential value in the treatment of cardiac hypertrophy partly through activation of the LKB1-AMPK pathway.

Keywords: cardiac hypertrophy; SIRT3; SZC-6; oxidative stress; mitochondrial malfunction; LKB1-AMPK pathway

Acta Pharmacologica Sinica (2023) 44:546–560; https://doi.org/10.1038/s41401-022-00966-8

INTRODUCTION

Cardiac hypertrophy is the adaptive enlargement of the heart resulting from increasing workload and is defined by an increase in the size of individual cardiomyocytes as well as overall organ hypertrophy. Although cardiac hypertrophy may be compensatory at first, it develops pathologically as heart failure progresses [1, 2]. The expression of pro-and anti-hypertrophic molecules is unbalanced at the molecular level, resulting in excessive protein synthesis and increased sarcomere structure. Our previous work has proven that mitochondrial deacetylase sirtuin 3 (SIRT3) is one of the anti-hypertrophic molecules and that deficiency promotes hypertrophy [3]. SIRT3 controls mitochondrial metabolism and energy synthesis in response to calorie restriction and metabolic stress, which confers its cardioprotective properties [4, 5]. Therefore, high-affinity small-molecule agonists targeting SIRT3 are expected to reduce the detrimental effects of pathological hypertrophy on cardiac energy metabolism.

Acetylation (Kac) is the most studied post-translational modification (PTM) of lysine. It is now obvious that reversible acetylation is a crucial regulatory mechanism for a variety of cellular proteins, and a significant proportion of acetylated proteins are mitochondrial metabolic enzymes [6, 7]. Sirtuins, a group of nicotinamide adenine dinucleotide (NAD^+)-dependent adenosine diphosphate (ADP)-ribosyltransferases and protein deacetylases, play important roles in the metabolism, stress, and aging [8, 9]. Research reports that three sirtuins (SIRT3, SIRT4 and SIRT5) are located in the mitochondria of seven mammalian sirtuins [10]. Among them, SIRT3 is the major mitochondrial deacetylase that modulates global alterations in cellular metabolism [11–13]. SIRT3 improves the efficiency of the tricarboxylic acid (TCA) cycle and the electron transport chain while mitigating oxidative stress to shield cells from harm [14].

SIRT3 deficiency results in decreased cellular adenosine triphosphate (ATP) [15–17]. During fasting, mice lacking SIRT3 show signs of abnormal fatty acid oxidation, such as a decrease in ATP levels and intolerance to low temperatures [18]. In addition, it has been reported that SIRT3 expression is reduced in the skeletal muscle of streptozotocin-diabetic mice, implying that SIRT3 is implicated in insulin signaling and the pathogenesis of diabetes [19, 20]. Similarly, cardiovascular disease risk factors reduce SIRT3 levels, and SIRT3 levels decline with age, paralleling the rising prevalence of cardiovascular disease and hypertension. These findings imply that promoting intracellular SIRT3 expression and activity can serve as a strategy to treat a variety of health-related disorders and deficiencies, such as cardiovascular diseases and diabetes.

[1]National-Local Joint Engineering Laboratory of Druggability and New Drugs Evaluation, Guangdong Province Engineering Laboratoty for Druggability and New Drug Evaluation, School of Pharmaceutical Sciences, Sun Yat-sen University, Guangzhou 510006, China and [2]School of Pharmaceutical Sciences, Sun Yat-sen University, Guangzhou 510006, China
Correspondence: Yong Zou (zouyong3@mail.sysu.edu.cn) or Pei-qing Liu (liupq@mail.sysu.edu.cn)

Received: 19 March 2022 Accepted: 24 July 2022
Published online: 30 August 2022

Several SIRT3 agonists derived from the natural product have shown promise in the treatment of cardiac hypertrophy and acute renal damage. Silybin is a liver protectant in traditional Chinese medicine, extracted from milk thistle seeds [21]. Upregulation of SIRT3 by silybin removes reactive oxygen species (ROS) and suppresses apoptosis, protecting kidney cells from death. Therefore, silybin can assist with clinical adjuvant treatment in cisplatin chemotherapy [22]. Likewise, Honokiol (HKL), derived from magnolia wood, can activate SIRT3 and protect tumor-xenograft mice from doxorubicin-induced cardiotoxicity without diminishing doxorubicin's antitumor effects, which indicating that HKL may have potential benefits as an adjunct to chemotherapy to alleviate the deleterious effects of chemotherapy [23]. According to current research, HKL stimulates SIRT3 to deacetylate manganese superoxide dismutase (MnSOD) and oligomycin sensitivity conferring protein (OSCP), reducing ROS generation, increasing mitochondrial oxygen consumption, and to some extent reducing myocardial remodeling [24]. Besides that, SIRT3 activation by HKL improves mitochondrial function and activates macroautophagy/autophagy to boost anti-mycobacterial responses via peroxisome proliferator-activated receptor alpha (PPARA-α) [4]. Furthermore, in AO-treated primary hippocampal neurons, HKL reduces synaptic damage, mitochondrial dysfunction, mitophagy and unfolded protein response in a SIRT3-dependent manner, highlighting HKL's anti-Alzheimer's disease effect [25].

To our knowledge, 7-hydroxy-3-(4-methoxyphenyl)-2H-chromen-2-one (C12) is the first SIRT3 agonist developed based on the crystal structure of the MnsodK68AcK-SIRT3 complex [1], containing a typical 3-arylcoumarin core. Taking C12 as the lead compound, further structural optimization of C12 was necessary for the development of novel SIRT3 agonists. Therefore, based on the 3-arylcoumarin core structure and the allosite binding pocket of SIRT3, modifications on the substituents have been made, which led to the discovery of SZC-6 with a reduced EC_{50} and K_d value, as well as better water solubility. Structurally, SZC-6 and C12 both share a common 7-hydroxy-3-arylcoumarin core, whereas differ in the substitutional pattern at ring C (2-bromated and 4-hydroxylated for SZC-6 vs. 4-methoxylated for C12). SZC-6 directly activated SIRT3 deacetylation by enhancing SIRT3's catalytic effect. Our results also revealed that SZC-6-mediated SIRT3 activation suppresses the heart hypertrophic responses in vitro and in vivo, which may help researchers to clarify SIRT3 deacetylation in more pathological conditions.

MATERIALS AND METHODS

Study animal

Jackson Laboratory provided male SIRT3-knockout (129-SIRT3tm1.1Fwa/J) mice and their wild-type (129/SvlmJ) controls (Bar Harbor, ME, USA). The Guangzhou University of Chinese Medicine Experimental Animal Center provided C57B/L6 mice (male, 9–12 weeks, certification No. 44008500024147) (Guangzhou, China). Sun Yat-sen University's Research Ethics Committee approved all surgical and care procedures. The mice were maintained in individually ventilated cages with 12 h daylight/dark cycles at 21–23 °C in a pathogen-free environment. The animals were fed conventional laboratory chow and had plenty of water available to them.

Histological examination and echocardiography

Mice were sedated with 3% isoflurane (*v/v*), and two dimensional-guided M-mode echocardiography was performed using a Technos MPX ultrasound system (Esaote, Genoa, Italy), as described in earlier investigations [26, 27]. The images were taken in M-mode and in 2D parasternal short-axis. Ejection fraction (EF), fractional shortening (FS), diastolic and systolic left ventricular posterior wall thickness (LVPW,d and LVPW,s), left ventricular internal dimensions (LVID,d and LVID,s), and left ventricular volume (LV Vol,d and LV Vol,s) were all calculated. All animals were then sacrificed as a result of this. For morphometric measurements, the hearts were stopped at end-diastole with a 0.1 mM KCl solution, fixed in 4% paraformaldehyde, and then calcinated.

Cell culture

Primary cultures of neonatal rat cardiomyocytes (NRCMs) were created using cells taken from the hearts of SD rats (1–2 days old) and identified using a specific test, as previously described [28]. Purified cardiomyocytes were seeded at a density of 1×10^6 cells per well into six-well plates, then maintained at 37 °C with 5% CO_2 in DMEM supplemented with 10% FBS and 5-bromodeoxyuridine in DMEM supplemented with 10% FBS and 5-bromodeoxyuridine (0.1 mM). After 48 h, NRCMs were administered isoprerenol or another stimulus before being incubated in serum-free medium for 24 h.

Western blot

SDS-polyacrylamide gel electrophoresis was used to separate equal amounts of total or mitochondrial protein, which was subsequently transferred to polyvinylidene fluoride membranes. The membranes were incubated with primary antibodies overnight at 4 °C before being exposed for 1 h to the appropriate secondary antibodies. The proteins were seen using enhanced chemiluminescence (Tanon, Shanghai, China).

Measurement of cell surface area

After being fixed with 4% paraformaldehyde for 20 min at room temperature, cardiomyocytes were sown in 24-well plates and treated with 0.1% Triton X-100 for 5 min. After 1 h of incubation with 0.2% rhodamine phalloidin, the cells were washed with HBSS and stained with DAPI (Invitrogen, Carlsbad, CA, USA). The cell surface area was determined using installed image processing software from randomly picked fields utilizing a Screening System (Arrayscan VTi 600 Plus, Thermo Scientific, San Jose, CA, USA) (30 for each group).

RNA extraction and quantitative real-time PCR (qRT-PCR)

The TRIzol reagent was used to extract total RNA from rat cardiac tissues or primary cell cultures (Takara Biotechnology, Dalian, China), and 1 g of total RNA was reverse-transcribed with the First Strand cDNA Synthesis Kit (Takara Biotechnology, Dalian, China) (Thermo Fisher Scientific, USA). On an ABI7500 real-time PCR equipment (Applied Biosystems, Foster, CA, USA), PCR was done using Master Mix (Takara, Dalian, China). The 2^{-Ct} technique was used to determine the relative expression level.

siRNA infection

siRNA were synthesized by GENECHEM (Shanghai, China). Cardiomyocytes were transfected with siRNA using TransIntro EL transfection reagent (TransGen Biotech, Beijing, China). Following the manufacturer's protocol for 72 h before harvest. The sequence of siRNA-AMPKα1/2, siRNA-LKB1, siRNA-SIRT3, and control siRNA are shown in Supplementary Table S2.

Dual-luciferase reporter assay

Cardiomyocytes were infected with a luciferase reporter plasmid harboring numerous NFAT-binding sites for the NFAT luciferase test. Cells were treated for 24 h with ISO (10 μM) in the presence or absence of SZC-6 24 h after infection. The SZC-6 treatment was given 12 h before the agonist treatment. The Luciferase activity assay was carried out using the Luciferase activity assay kit (Yeason, Shanghai, China). Lipofectamine 2000 was used for all transfections (Invitrogen, Carlsbad, CA, USA).

Measurement of mitochondrial oxygen consumption rate (OCR)

As previously published, OCR was measured using an XF96 Extracellular Flux Analyzer (Seahorse Bioscience, North Billerica,

MA, USA) [29]. H9c2 cells were seeded at a density of 5×10^4 cells/well in Seahorse XF96 microplates (Seahorse Bioscience, North Billerica, MA, USA) for 24 h in a 37 °C incubator with 5% CO_2 (DMEM). The cells' regular medium was then changed with XF assay medium, which had 1 nM pyruvate, 10 mM glucose, and 2 mM glutamine. The following substances were used to fill a sensor cartridge: oligomycin (2 M), carbonylcyanide 4-(trifluoromethoxy) phenylhydrazone (FCCP, 1 M), and rotenone/antimycin A (1 M). The cell plates were incubated in a 37 °C/non-CO_2 incubator for 60 min prior to the start of the OCR test after the sensor cartridge was calibrated in the analyzer. The OCR was normalized using the cell count in each well. The data were analyzed with Wave software, and respiratory parameters were quantified. At least three times, the experiment was carried out.

Determination of mitochondrial membrane potential (ΔΨm) and ATP production

The methyl ester of tetramethylrodhamine was used to determine the mitochondrial membrane potential (TMRM, Invitrogen, Carlsbad, CA, USA). Cardiomyocytes were collected, washed, and resuspended in PBS, in a nutshell. After that, cells were loaded with 200 nM TMRM in PBS for 20 min at 37 °C. A FACScan flow cytometer was used to assess the cells after they had been washed (Beckman Coulter, Indianapolis, IN, USA). A total of 10,000 occurrences were captured in each analysis. A luciferase-based assay kit was used to assess the amounts of ATP in NRCMs (Beyotime, Shanghai, China). NRCMs were lysed to extract ATP from the cells in a nutshell. Based on the ATP and luciferase responses, the ATP level was evaluated using a mix of ATP detection solution and luciferase solution. The concentration was adjusted to match the cellular protein concentration. The final outcomes were revealed. The final percentage of the control group was presented.

Mitochondrial fission analysis

NRCMs were treated with or without SZC-6 (10 μM) for 24 h for the mitochondrial fission assay. After treatment, the cells were washed in PBS and then incubated for 30 min at 37 °C with 300 nmol/L Mito Tracker red (Molecular Probes, Eugene, OR, USA). Confocal microscopy was used to examine the structure of mitochondria. The percentage of cells undergoing mitochondrial fission was calculated from 90 cells in three separate studies. The detection and statistics of mitochondrial length were carried out as previously reported [30].

Transmission electron microscopy (TEM)

To determine the structure of mitochondria morphologically, ultrastructure analysis was conducted out as previously reported. The heart tissue was initially sliced into 1 mm^3 patches and treated with ice-cold glutaraldehyde at a concentration of 2.5% (Solarbio, Beijing, China). After being washed in PBS, all samples were implanted in epoxy resin after being post-fixed with OsO_4 (Electron Microscopy Sciences, Hatfield, PA, USA). Uranyl acetate (E. Merck, Darmstadt, Germany) and lead citrate were used to stain ultrathin slices (Sigma-Aldrich, St. Louis, MO, USA). For observation, a transmission electron microscope (JEM-100CXII, Japan) was employed. The entire procedure was carried out with the observer obscured from view.

Materials

Primary antibodies against SIRT3 (Cat# 5490), Drp1 (Cat# 14647), Phospho-DRP1 (Ser616) (Cat# 3455), Phospho-AMPKα (Thr172) (Cat# 2535), AMPK (Cat# 5831) and Acetylated-Lysine (Cat# 9441) were obtained from Cell Signaling Technology. Antibodies against LKB1 (sc-32245), Phospho-LKB1 (sc-271924), ACC (sc-137104), and Phospho-ACC (sc-271965) were purchased from Santa Cruz Biotechnology (Dallas, TX, USA). Beta-MHC antibody was obtained from Sigma-Aldrich. GAPDH (Cat# 60004-1-AP), Mfn2 (Cat# 12186-1-AP), NAMPT (Cat# 11776-1-AP), OPA1 (Cat# 27733-1-AP), SIRT1 (Cat# 13161-1-AP) and Mnsod (Cat# 24127-1-AP) bodies were purchased from Proteintech Group (Manchester, UK). An Acetyl-SOD2 antibody was purchased from Affinity Biologicals (Hamilton, ON, USA).

Statistical analysis

The data are expressed as the mean ± SEM of multiple independent replicates. The statistical analyses included two-tailed, unpaired Student's *t* tests for experiments with two groups or one-way ANOVA with Bonferroni posttests for multiple groups (GraphPad Prism 9.0 software, San Diego, CA, USA). Statistical significance was defined as $P < 0.05$.

RESULTS

Discovery of selective SIRT3 activators

In comparison to orthosteric ligands, allosteric ligands had higher selectivity and better physio-chemical properties, which enabled them to modulate difficult pharmacological targets. The exact identification of allosteric sites was a precondition for allosteric drug design. Given the challenges in pharmacologically activation of SIRT3, we predicted allosteric sites in SIRT3 by using the Allosite method developed by Zhang's group [31]. According to the forecasts, a pocket would form around Phe180 and Phe294 on the surface of SIRT3, which could serve as allosteric sites (Fig. 1a). To find possible SIRT3 activators, we used a combination of computational and experimental methods. Afterwards, we virtually docked over 2000 molecules into the anticipated location and then selected and synthesized 33 of them on the basis of the top-ranked SIRT3 compound binding models. The SIRT3 Deacetylase Fluorometric Assay kit (Cyclex) was used to test the ability of these compounds to agonize SIRT3 in vitro (Supplementary Fig. S1). Two of these 33 compounds hit, C12 and SZC-6 (Fig. 1b). The chemical synthetic route was shown (Supplementary Figs. S10–17). SIRT3 had a two-domain structure, a binding site for a Rossmann fold domain that bound NAD^+ with a zinc binding motif, and a smaller domain with a helical bundle. The docking studies revealed that C12 had the potential to generate H-bonds with Ile230, Asn229 and Phe180 of SIRT3. However, the hydroxy phenyl ring of the SZC-6 penetrated deep into the cleft between the two domains and formed arene-arene stacking with His248, which was critical for the deacetylation activity of sirtuins and absolutely conserved in SIRT1-7 (Fig. 1c), and Phe180 formed H-bonds with Asn229.

To test the binding affinity between SZC-6, C12 and SIRT3, we used a surface plasmon resonance (SPR) assay. C12 bound SIRT3 in a dose-dependent manner (the equilibrium dissociation constant $[K_d] = 24.3$ μM) (Fig. 1d). SZC-6 also bound directly to SIRT3 in a concentration-dependent manner ($[K_d] = 15$ μM) (Fig. 1e). We further assessed SZC-6 and C12's potential to directly agonize SIRT3's deacetylase activity to calculate EC_{50} values for concentration-response curves. Our results indicated that SZC-6 and C12 increased SIRT3 deacetylation activity with EC_{50} values of 23.2 ± 3.3 μM and 71.8 ± 5.3 μM, respectively. Both compounds considerably increased SIRT3 deacetylation activity by more than 20-fold at 100 μM (Fig. 1f). These results suggested that SZC-6 had a better capability to agonize SIRT3 activity and higher selectivity than C12. This could be related to the unique binding site of SIRT3, which caused a conformational change in SIRT3 that favored NAD^+ binding and deacetylation activity.

SZC-6 enhances the deacetylase activity of SIRT3

SIRT3, a deacetylase mainly present in mitochondria, was closely linked to oxidative stress and has been implicated in cardiac disorder [20]. To test SIRT3 activators, the study examined the acetylation status of mitochondrial proteins in cardiomyocytes after treatment with different doses of SZC-6. Treatment of

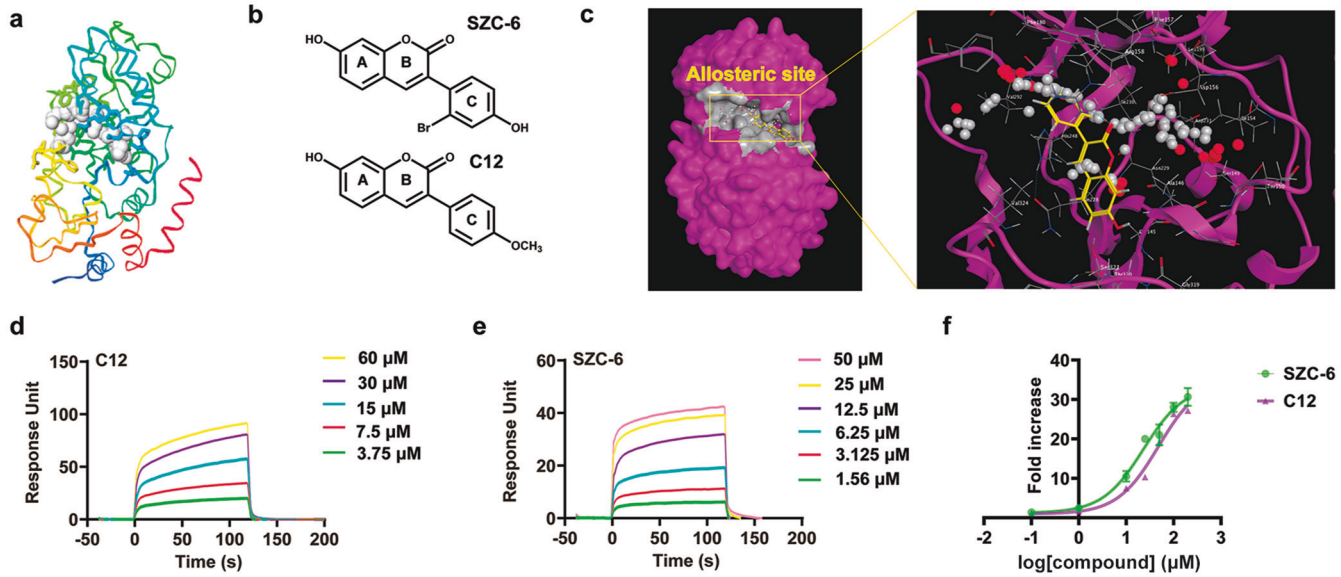

Fig. 1 SZC-6 bound to an allosteric site of SIRT3. a The superposition of full-length SIRT3 with the predicted allosteric pocket. Residues in the pocket are shown in gray. **b** Chemical structures of SZC-6. **c** Predicted cocrystal structure of SZC-6 in connection with SIRT3. Left, overall structure with SIRT3's surface colored in violet. Right, magnified view of the allosteric site of SZC-6. SIRT3 is displayed as a violet cartoon, and SZC-6 is shown in sticks. Dotted lines are used to represent hydrogen bonding. **d**, **e** Surface plasmon resonance (SPR) analysis for the binding effects of C12 and SZC-6 on SIRT3. The compound and substrate peptide used in SPR are labeled in each panel. **f** Dose-dependent effects of SZC-6 and C12 on SIRT3, determined with fluorimetric activity assays. Data are presented as mean ± SEM, $n = 3$.

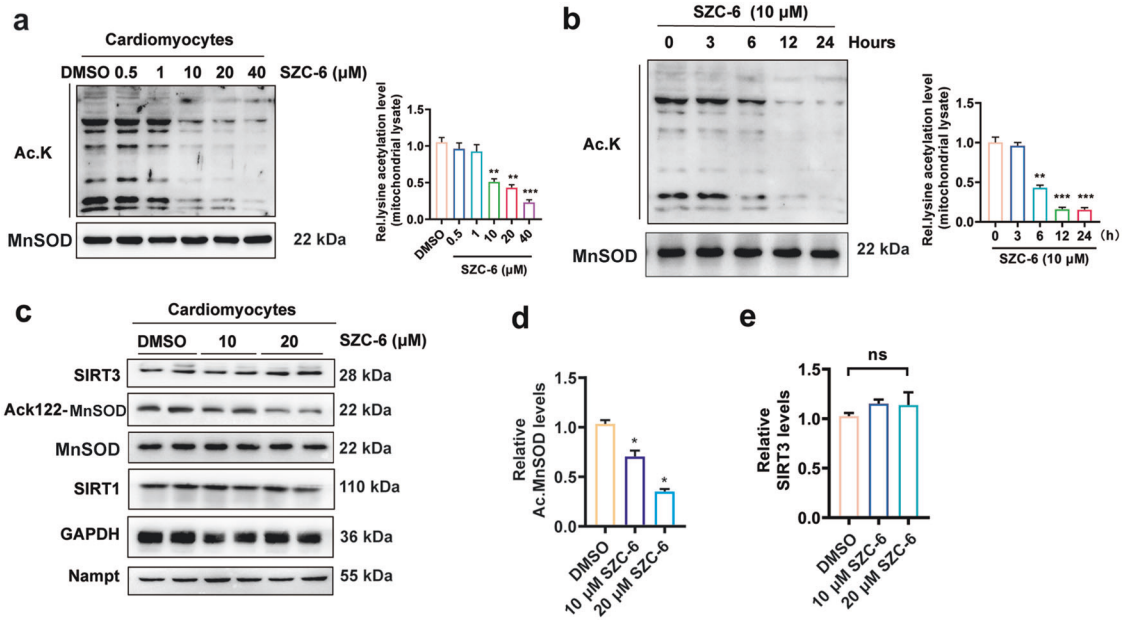

Fig. 2 SZC-6 activates SIRT3 and deacetylates mitochondrial proteins. a SZC-6 was used to treat primary cultures of neonatal rat cardiomyocytes at various dosages, as shown. An anti-acetyl lysine antibody was used to examine mitochondrial lysate for lysine acetylation. Manganese superoxide dismutase (MnSOD) served as the loading control. The data are presented as the mean ± SEM. $^{**}P < 0.01$, $^{***}P < 0.001$, *vs*. the DMSO group; $n = 4$. **b** Cardiomyocytes were treated with 10 μM or 20 μM SZC-6 for 24 h. appropriate antibodies was used to examine the cell lysate. The data are presented as the mean ± SEM. $^{**}P < 0.01$, $^{***}P < 0.001$, *vs*. the DMSO group; $n = 4$. **c** Neonatal rat cardiomyocytes were treated with 10 μM SZC-6 at various time points. Mitochondrial lysate was produced and lysine-acetylation was determined. **d**, **e** The acetylation of MnSOD at lysine (K) 122 (Ack122-MnSOD) and expression of SIRT3 in cardiomyocytes treated with SZC-6 was detected by Western blot analysis. The data are presented as mean ± SEM. $^{*}P < 0.05$, $^{**}P < 0.01$, $^{***}P < 0.001$ *vs*. the DMSO group; $n = 4$.

cardiomyocytes with SZC-6 resulted in a dose-dependent reduction in mitochondrial protein acetylation (Fig. 2a), which was consistent with the deacetylase activity assay of SZC-6 tested in vitro. Based on our optimized concentration of SZC-6, cardiomyocytes were treated with 10 μM SZC-6 for various lengths of time and the acetylation status of mitochondrial proteins was analyzed. SZC-6 could diminish mitochondrial acetylation with increasing duration at 10 μM (Fig. 2b), indicating increased SIRT3 activity. SIRT3 has been found to increase Mnsod's enzymatic activity by deacetylating it at K-122. We determined the

acetylation status of the MnSOD by using antibodies that exclusively detect MnSOD acetylation at K-122. It was found that MnSOD acetylation was reduced after SZC-6 therapy, indicating the increase of SIRT3 activity (Fig. 2c, d). We then explored whether the activation of SIRT3 was attributable to the increased cellular levels of SIRT3 following SZC-6 treatment. SIRT3 levels were further analyzed by immunoblotting. Data analysis revealed that SZC-6 treatment had a much greater influence on SIRT3 activity, which was independent of its protein levels (Fig. 2c, e). Nampt was reported to promote mitochondrial biogenesis and function in conjunction with SIRT3 [32]. Moreover, SIRT1 and SIRT3 shared a common mechanism and similar substrate preferences, regulating the acetylation of both histones and other cellular proteins in an NAD^+-dependent manner [33]. Nampt was a crucial component of the mitochondrial NAD^+ salvage pathway that stimulated SIRT3 to facilitate cell survival [34]. Thereafter, we examined the effects of SZC-6 on SIRT1 and Nampt, but found no significant differences (Fig. 2c). Therefore, SZC-6 activated endogenous SIRT3 deacetylation in cardiomyocytes.

SZC-6 attenuates hypertrophic response of cardiomyocytes in vitro

According to previous findings, SIRT3 protected cardiomyocytes from hypertrophic stress [35, 36]. It was further investigated whether SZC-6 treatment could protect cardiomyocytes from developing cardiac hypertrophy. Cardiomyocytes were treated with isoproterenol (ISO) in the presence or absence of SZC-6 at doses of 10, 20 and 40 μM. The cardiomyocyte hypertrophy was monitored by measuring cell surface area and the expression levels of ANF, BNP and β-MHC, which were biomarkers of the hypertrophic response. The results demonstrated that SZC-6 suppressed the enlargement of neonatal rat cardiomyocytes (NRCMs) induced by ISO (Fig. 3a). In addition, it revealed that ISO stimulation-induced upregulation of β-MHC, ANF, and BNP expression was inhibited by SZC-6 treatment in a dose-dependent manner with maximum effects at 40 μM (Fig. 3b, d, e). However, the pretreatment of SZC-6 did not change the expression level of SIRT3 at different doses (Fig. 3c). Translocation of nuclear factor of activated T cells (NFAT) into the nucleus was known to occur in response to hypertrophic stimuli, resulting in increased NFAT transcriptional activity that was important in cardiac hypertrophy [37]. Cardiomyocytes were transiently co-transfected with an NFAT luciferase reporter plasmid and treated with ISO in the presence or absence of 10 μM SZC-6 to see if SZC-6 could prevent ISO-induced NFAT activation. The ISO-induced activation of the NFAT-reporter gene was blocked by SZC-6 treatment (Fig. 3f). Collectively, SZC-6 appeared to be capable of suppressing the hypertrophic cardiac response in vitro.

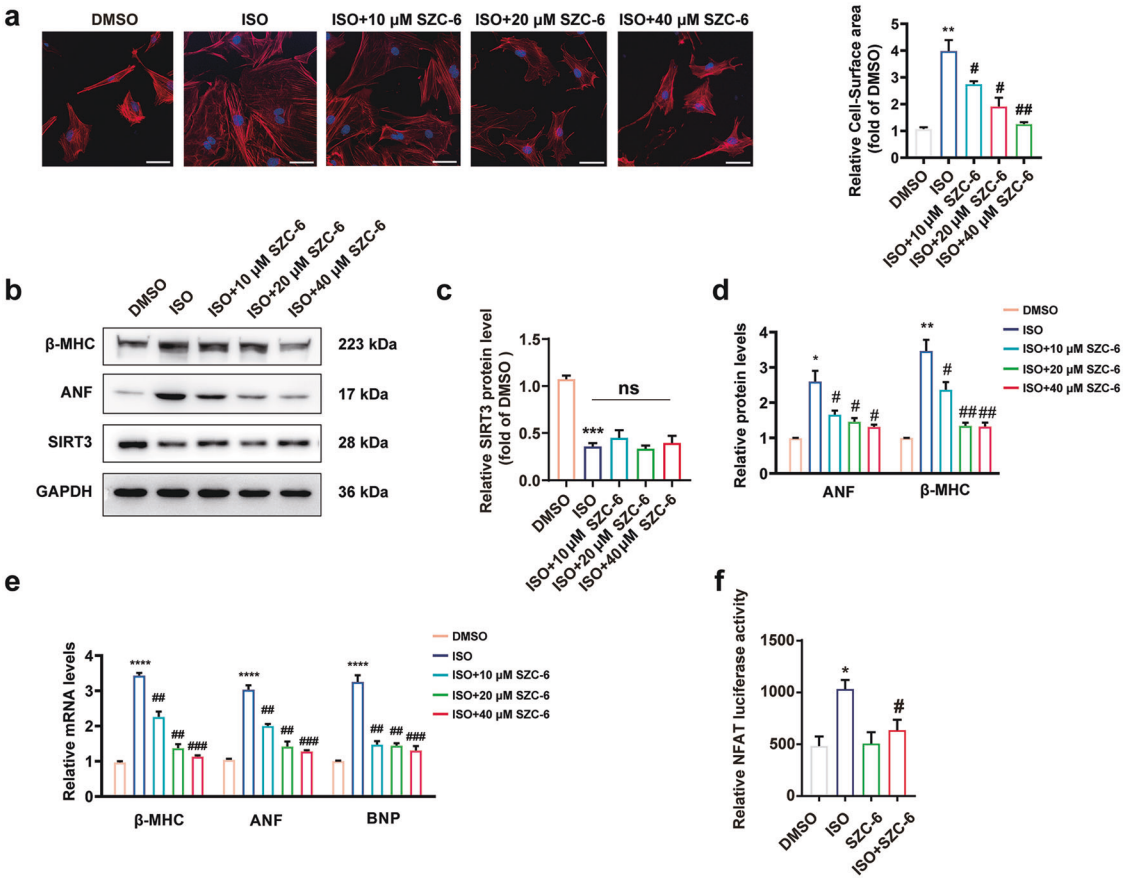

Fig. 3 SZC-6 attenuates stress-induced hypertrophic responses in cardiomyocytes in a dose-dependent manner. NRCMs were pretreated with SZC-6 for 24 h or DMSO followed by incubation with ISO (10 μM for 24 h). **a** The surface area of NRCMs was measured (Scale bar = 20 μm). The data are presented as the mean ± SEM. $^{**}P < 0.01$ *vs.* the DMSO group; $^{\#}P < 0.01$, $^{\#\#}P < 0.01$ *vs.* the ISO group; $n = 4$. **b**, **d** The protein expression of ANF and β-MHC was detected by Western blot analysis. The data are presented as the mean ± SEM. $^{*}P < 0.05$, $^{**}P < 0.01$ *vs.* the DMSO group; $^{\#}P < 0.05$, $^{\#\#}P < 0.01$ *vs.* the ISO group; $n = 4$. **c** The protein expression of SIRT3 was detected by Western blot analysis. The data are presented as the mean ± SEM. $^{***}P < 0.001$ *vs.* the DMSO group. $n = 4$. **e** The mRNA levels of β-MHC, ANF and BNP in NRCMs were measured by qRT-PCR. The data are presented as the mean ± SEM. $^{****}P < 0.0001$ *vs.* the DMSO group; $^{\#\#}P < 0.01$, $^{\#\#\#}P < 0.001$ *vs.* the ISO group; $n = 4$. **f** H9c2 cells were transfected with a NFAT-responsive luciferase reporter plasmid. Cells (24 h after infection) were treated with ISO in the presence or absence of 10 μM SZC-6 for 24 h, and luciferase activity was detected. The data are presented as the mean ± SEM. $^{*}P < 0.05$ *vs.* the DMSO group; $^{\#}P < 0.05$ *vs.* the ISO group; $n = 3$.

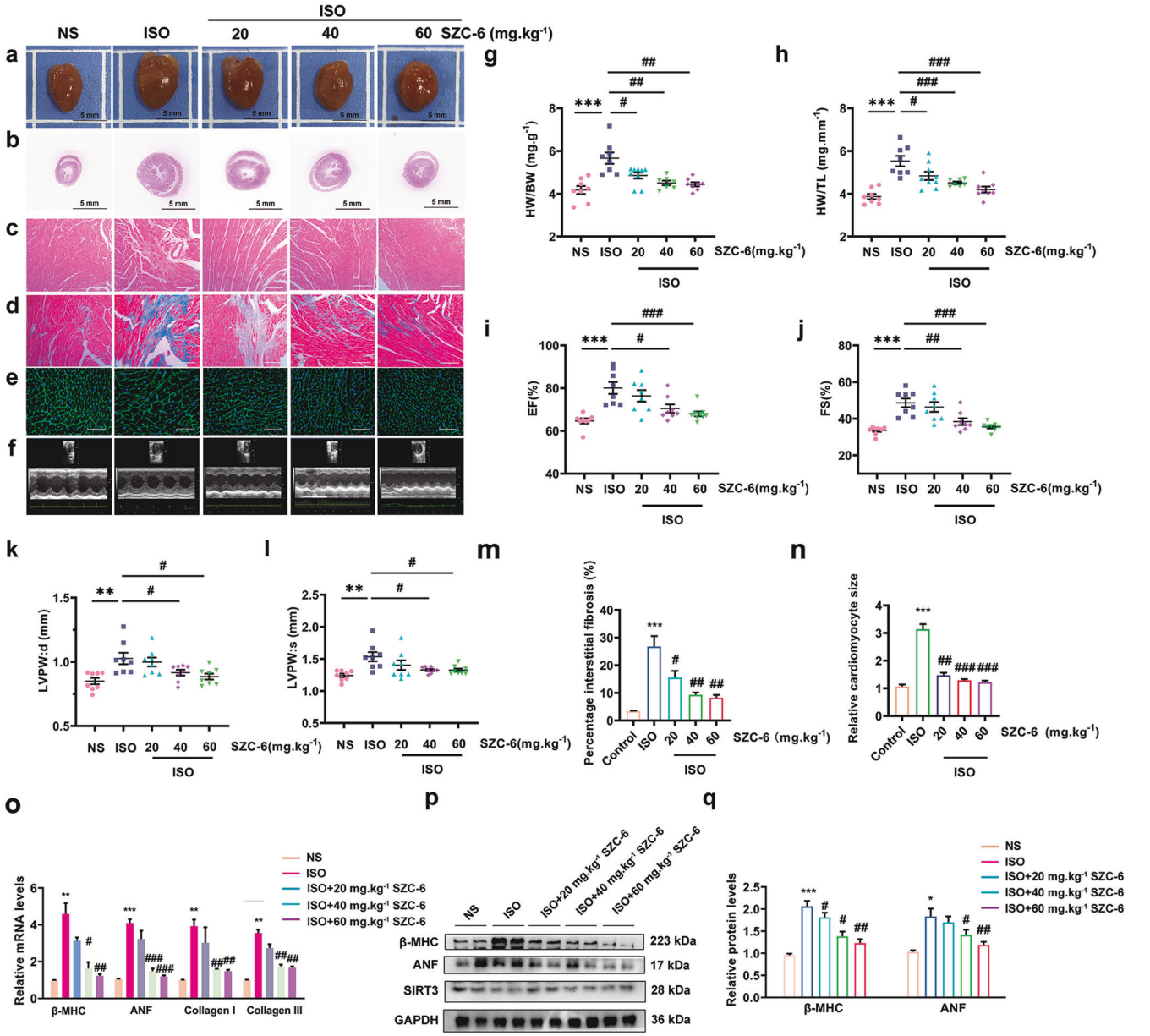

Fig. 4 Pretreatment with SZC-6 blunts cardiac hypertrophy in vivo. C57B/L6 mice were subcutaneously infused with SZC-6 or normal saline (NS) for 1 week and then subjected to injections of ISO with SZC-6 or normal saline (NS) for 1 week. The pathological changes in the myocardium were observed. **a** gross morphologic examination. H&E staining (**b**, scale bar = 5 mm; **c**, scale bar = 200 μm). **d** Heart sections stained with Masson's trichrome to detect fibrosis (scale bar = 200 μm). **e** WGA staining (scale bar = 50 μm). **f** Echocardiography. **g**, **h** The HW/BW ratio and HW/TL ratio were calculated. **i**–**l** Echocardiographic parameters were measured. The data are presented as the mean ± SEM. $^{**}P < 0.01$, $^{***}P < 0.001$ *vs.* NS; $^{\#}P < 0.05$, $^{\#\#}P < 0.01$, $^{\#\#\#}P < 0.001$ *vs.* ISO; $n = 8$–9. **m**, **n** Quantification of cardiac fibrosis and myocyte cross-sectional area in different groups of mice. The data are presented as the mean ± SEM. $^{***}P < 0.001$ *vs.* the NS group; $^{\#}P < 0.05$, $^{\#\#}P < 0.01$, $^{\#\#\#}P < 0.001$ *vs.* the ISO group; $n = 4$. **o**–**q** The protein and mRNA levels of β-MHC, ANF, Collagen I, Collagen III and SIRT3 in cardiac tissues were measured by Western blot analysis and qRT-PCR. The data are presented as the mean ± SEM. $^{**}P < 0.01$, $^{***}P < 0.001$ *vs.* the NS group; $^{\#}P < 0.05$, $^{\#\#}P < 0.01$, $^{\#\#\#}P < 0.001$ *vs.* the ISO group; $n = 4$.

SZC-6 repressed ISO-induced cardiac hypertrophy in vivo

In order to evaluate the physiological significance of studies in vitro, the efficacy of SZC-6 to prevent the development of heart hypertrophy in vivo was then investigated. We used three different doses of SZC-6 to test the dose-response relationships. Three doses of 20, 40 and 60 mg·kg^{-1}·d^{-1} SZC-6 were given for 1 week, and then mice were injected with ISO (5 mg·kg^{-1}·d^{-1}) and different doses of SZC-6 for 7 days. According to morphologic and histological investigations, the most obvious protective effect against hypertrophy occurred at the highest dose level of 60 mg·kg^{-1}·d^{-1} (Fig. 4a–f). SZC-6 decreased ISO-stimulated pathological alterations associated with hypertrophy, as demonstrated by lower HW/BW ratio, HW/TL ratio, and echocardiographic measures such as EF, FS, LVPW (Fig. 4g–i). A lower E/A ratio measured by Doppler imaging suggested impaired diastolic function in the ISO group. SZC-6 ameliorated diastolic function by restoring E/A index (Supplementary Fig. S2). The accumulation of collagen fibers was also obviously reduced, which was detected by Masson staining and evaluation (Fig. 4m), suggesting that SZC-6 also had anti-fibrotic effects. The inhibitory impact of SZC-6 on hypertrophic development in mice was further validated using wheat germ agglutinin (WGA) staining (Fig. 4n). The expression of

hypertrophic markers such as ANF, BNP, Collagen I, Collagen III and β-MHC in cardiac tissues from ISO-infused animals were reduced by SZC-6 in a dose-dependent manner (Fig. 4o–q). These results demonstrated that SZC-6 could protect against ISO-triggered cardiac hypertrophy in vivo.

SIRT3 mediates anti-hypertrophic activity of SZC-6

To demonstrate that SZC-6's anti-hypertrophic effects were mediated by SIRT3 activation, SIRT3 was knocked down in NRCMs using RNA interference. SZC-6 clearly inhibited the hypertrophic response induced by ISO, as evidenced by a decrease in ANF and β-MHC protein levels. However, this effect was blunted by the small interfering RNA (siRNA) targeting SIRT3 but not by the control siRNA (Fig. 5a). To further confirm that the anti-hypertrophic effect of SZC-6 is mediated by SIRT3, we administered SZC-6 (60 $mg{\cdot}kg^{-1}{\cdot}d^{-1}$) for 1 week and then subjected the male SIRT3-KO mice and their wild-type (WT) littermates to injections of ISO (5 $mg{\cdot}kg^{-1}{\cdot}d^{-1}$) and SZC-6 (60 $mg{\cdot}kg^{-1}{\cdot}d^{-1}$) for 7 days. It was worth noting that the ISO-induced deterioration in cardiac function was exacerbated in KO mice compared to the wild-type mice. In addition, we measured the effect of SZC-6 in SIRT3-deficient hearts. It was also seen that both SZC-6-treated and untreated SIRT3-KO mice had markedly elevated hypertrophic responses with the results of gross morphologic examination, H&E staining, echocardiography, the HW/BW and HW/TL ratios, and the expression of hypertrophic marker genes (Fig. 5b–r). These results implied that SZC-6 was unable to block hypertrophic response in SIRT3-KO hearts, whereas it blocked hypertrophic response in the hearts of wild-type mice. SZC-6 therapy also reduced MnSOD acetylation in wild-type mice, but not in SIRT3-KO organisms (Supplementary Fig. S3). These above results showed that SIRT3-mediated signaling was involved in SZC-6's anti-hypertrophic activities.

SZC-6 blocks proliferation and differentiation of cardiac fibroblasts through SIRT3

A crucial process of human heart diseases was left ventricular hypertrophy, which was characterized by cellular (hypertrophy) and extracellular matrix enlargement (interstitial fibrosis) [38]. Therefore, Masson's trichrome staining displayed that the SZC-6 treated ISO group of wild-type mice had less ventricular fibrosis. In neonatal rat cardiac fibroblasts, ISO could induce the production of stress fiber and enhance the expression of smooth muscle alpha actin (SMA) and fibronectin. We next determined whether SZC-6 could prevent the transformation of cardiac fibroblasts into myofibroblasts by detecting the production of SMA and fibronectin which were considered key markers of myofibroblast differentiation. The fluorescence intensity of SMA and fibronectin was decreased when cells were treated with SZC-6, and this was also indicated by the protein levels of fibronectin and SMA (Fig. 6a–d), suggesting that SZC-6 attenuated fibroblasts differentiation into myofibroblasts. We also determined whether these anti-fibroblast effects of SZC-6 were mediated through SIRT3. Cardiac fibroblasts from wild-type and SIRT3-KO mice were extracted and treated with ISO in the presence or absence of 10 μM SZC-6. Fibronectin and SMA staining illustrated that SZC-6 failed to block ISO-induced differentiation of SIRT-KO fibroblasts, and SZC-6 had no effect on transformation of fibroblasts (Fig. 6e, g). The results of immunofluorescence staining were corroborated by Western blot analysis of the core protein (Fig. 6i), indicating that SZC-6 suppressed fibroblast development through activating SIRT3. Subsequently, we aimed to see if SZC-6 could stop cardiac fibroblasts from proliferating, which was an important fibrosis progress. To assess fibroblast proliferation, we used flow cytometry based on the quantification of EdU incorporation, a sign of cell proliferation. SZC-6 treatment reduced the proportion of S-phase cells in a dose-dependent manner, suggesting that SZC-6 could also blocked cardiac fibroblasts proliferation (Fig. 6f, h). These findings supported the idea that SIRT3 was involved in SZC-6's antifibrotic activities.

SZC-6 attenuates ISO-induced oxidative stress and mitochondrial dysfunction

Abnormal generation of ROS caused oxidative stress in the heart, which led to cardiac toxicity and hypertrophy [39]. Peroxisomes, endoplasmic reticulum, and mitochondria were the most common sources of cellular ROS [40, 41]. Therefore, we next sought to see if pre-treating cells with SZC-6 inhibited ROS production. Flow cytometry was used to quantify intracellular ROS using the DCFH-DA probe. Compared with the control group, ISO boosted ROS production by 60%. On the other hand, SZC-6 pre-treatment dramatically reduced ISO-induced ROS only in NRCMs treated with control siRNA (Fig. 7a, b). Considering the formation of ROS in mitochondria and the collapse of mitochondrial membrane potential were inextricably linked, we used the mitochondrial membrane potential dye, TMRE, to quantify mitochondrial membrane potential in NRCMs in subsequent investigations. However, it was found that the increase in mitochondrial membrane potential caused by SZC-6 treatment was reversed by the knockdown of SIRT3 expression (Fig. 7d, e). Changes in mitochondrial fusion and fission were tightly linked to ΔΨm as well as mitochondrial homogeneity. Mitochondria were dynamical organelles that required constant fission and fusion to stay functional [42]. Mitochondria fragments in response to stress or apoptotic activation, and this fragmentation may lead to permeabilization of mitochondrial outer membrane [43]. Therefore, the expression of mitochondrial fusion/fission proteins was determined both in vitro and in vivo. The ISO reduced the expression of mitofusin 2 (Mfn2) and increased the expression of dynamin-related peptide 1 (Drp1) in NRCMs, which was accompanied by an increase of Drp1-Ser616 phosphorylation in mitochondria fraction (Fig. 7c–h). SZC-6 was unable to reverse ISO-induced alterations in myocardial fusion/fission protein expression in SIRT3-KO mice, but it could do so in wild-type mice (Supplementary Fig. S4). SZC-6 therapy successfully reduced the ISO-induced alerted fusion/fission protein expression. Besides, the effect of SZC-6 on mitochondrial fission was further confirmed by MitoTracker Red staining, while SZC-6 prevented excessive fragmentation of mitochondria (Fig. 7j, i). Quantification of mitochondrial length showed the same result (Fig. 7m). Next, mitochondrial respiratory activity was assessed by determining oxygen consumption rates (OCRs) in H9c2 cells using a Seahorse XF96 Extracellular Flux Analyzer. The measurements of respiration parameters showed that the SZC-6 group had higher basal respiration, ATP generation, and maximal respiration than the control group. In contrast, inhibition of SIRT3 with 3-TYP decreased mitochondrial respiratory activity, as indicated by reduced respiration parameters (Fig. 7i, k). Additionally, the ATP levels in NRCMs were also measured by a luminometric assay using an ATP bioluminescent assay kit, the same trend was observed after SZC-6 treatment (Supplementary Fig. S5). Moreover, the effects of SZC-6 on mitochondrial morphology of mice cardiac tissues were further characterized by transmission electron microscope (TEM). The administration of SZC-6 to mice prevented ISO-induced mitochondrial swelling, cristae rupture and vacuolization, while this effect was blunted in the SIRT3-KO group (Fig. 7m). To summarize, SZC-6 therapy greatly reduced the effects of ISO on mitochondrial morphology.

SZC-6 improved mitochondrial function via the SIRT3-LKB1-AMPK pathway

AMP-activated protein kinase (AMPK), a protein that preserved heart muscle from damage during ischemia, was regulated by liver kinase B1 (LKB1) [44]. Moreover, it was reported that SIRT3 was required for maintaining LKB1 activity [45]. Through SIRT3 deletion, inhibition, and transfection of SIRT3 active site mutation

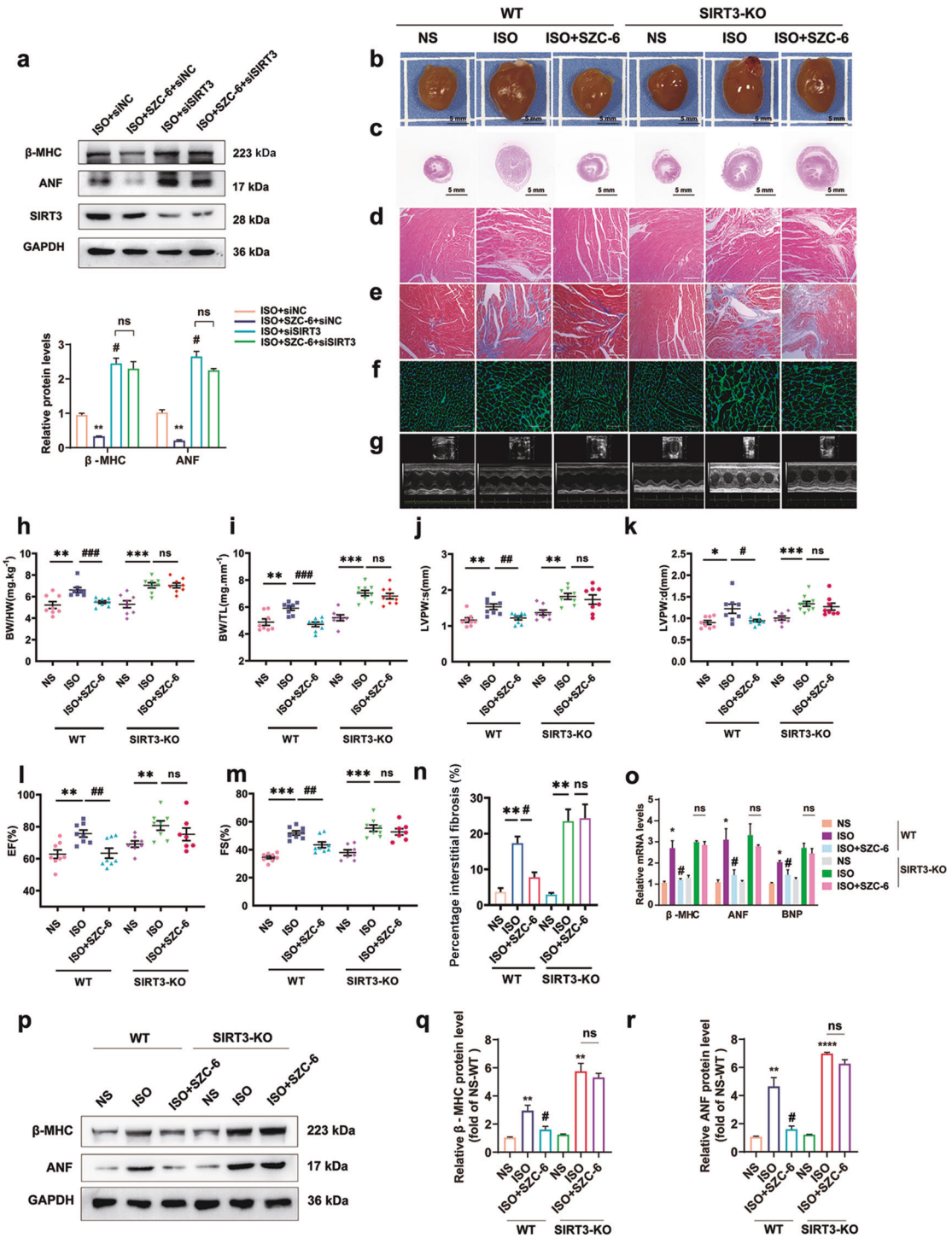

Fig. 5 SZC-6 treatment attenuates pathological hypertrophy of wild type, but not SIRT3-KO mice. SIRT3$^{-/-}$ mice and SIRT3$^{+/+}$ mice were subcutaneously infused with SZC-6 (60 mg·kg^{-1}·d^{-1}) or normal saline (NS) for 1 week and then subjected to injections of ISO with SZC-6 or normal saline (NS) for 1 week. The pathological changes of the myocardium were observed. **a** The protein expression of ANF, β-MHC and SIRT3 was detected by Western blot analysis. **b** Gross morphologic examination of the hearts. H&E staining of cardiac sections (**c**, scale bar = 5 mm; **d**, scale bar = 200 μm). **e** Heart sections stained with Masson's trichrome to detect fibrosis (scale bar = 200 μm). **f** WGA staining (scale bar = 50 μm). **g** Representative images of echocardiography. **h**, **i** The HW/BW ratio and HW/TL ratio were calculated. **j**–**m** Echocardiographic parameters were measured. The data are presented as the mean ± SEM. $^{**}P < 0.01$, $^{***}P < 0.001$; $^{\#\#}P < 0.01$, $^{\#\#\#}P < 0.001$; $n = 8$. **n** Quantification of cardiac fibrosis in different groups of mice. The data are presented as the mean ± SEM. $^{**}P < 0.01$, $^{***}P < 0.001$; $^{\#}P < 0.05$; $n = 4$. **o**–**r** The protein and mRNA levels of β-MHC, ANF and BNP in cardiac tissues were measured by Western blot analysis and qRT-PCR. The data are presented as the mean ± SEM. $^{*}P < 0.05$, $^{**}P < 0.01$, $^{***}P < 0.001$; $^{\#}P < 0.05$; $n = 4$.

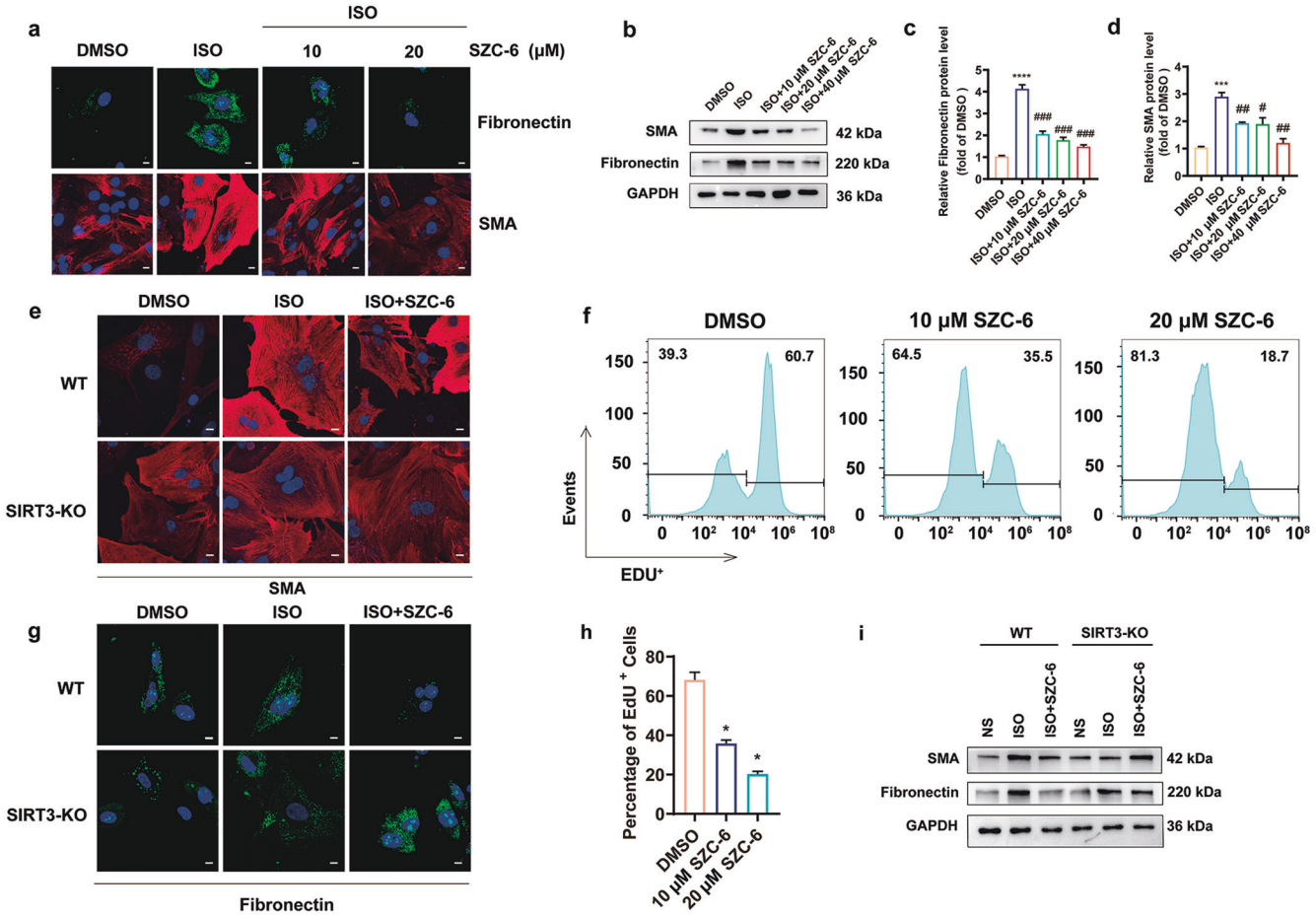

Fig. 6 SZC-6 attenuates cardiac fibroblasts proliferation and differentiation into myofibroblasts. a Primary cultures of rat cardiac fibroblasts were immunostained for SMA and fibronectin (scale bar = 10 μm). **b–d** Rat cardiac fibroblasts were treated with different doses of SZC-6 as indicated followed by incubation with ISO. The expression of SMA and fibronectin were detected by Western blot analysis. The data are presented as the mean ± SEM. $^{***}P < 0.001$, $^{****}P < 0.0001$; $^{\#}P < 0.05$, $^{\#\#}P < 0.01$, $^{\#\#\#}P < 0.001$; $n = 4$. **e**, **g** Primary cultures of mouse cardiac fibroblasts obtained from wild-type (WT) and SIRT3-KO mice were treated with 10 μM ISO in the presence or absence of SZC-6 for 24 h. Cells were immunostained for SMA and fibronectin (scale bar = 10 μm). **f** Rat cardiac fibroblasts were treated with 10 or 20 μM SZC-6. Cells (24 h after SZC-6 treatment) were treated with EDU for 1 h. Cells were harvested and subjected to fluorescence active cell sorter analysis (FACS). **h** Quantification of S-phase cells. mean ± SEM, $^{*}P < 0.05$ *vs.* the DMSO group; $n = 4$. **i** The protein levels of SMA and fibronectin in cardiac tissues were measured by Western blot analysis.

plasmids in NRCMs, it was confirmed that the deacetylase activity of SIRT3 could directly alter the phosphorylation of LKB1 (Supplementary Fig. S6). Then, we found that SZC-6 significantly enhanced LKB1 phosphorylation in a dose-dependent manner in NRCMs (Fig. 8a). The acylation of LKB1 was also detected in vivo. SZC-6 decreased the acylation of LKB1 only in wild-type mice (Fig. 8b), whereas knockdown of SIRT3 abolished SZC-6-induced phosphorylation of LKB1 in vivo (Fig. 8d). The results showed that SZC-6 notably increased LKB1 activation (phosphorylation). SZC-6 also elevated the binding between SIRT3 and LKB1, as indicated by the colocalization of SIRT3 and LKB1 in the immunofluorescence staining result. It was plausible that the interaction between SZC-6 and SIRT3's allosite pocket enhanced SIRT3 and LKB1 binding affinity in a synergistic way. Furthermore, the reduction of SIRT3 activity by 3-TYP affected LKB1-SIRT3 colocalization (Fig. 8c). This suggested that some increases in binding between SIRT3 and LKB1 by SZC-6 were dependent on the deacetylase activity of SIRT3. To understand if LKB1 was involved in the SZC-6-induced reversal of cardiac hypertrophy, we suppressed LKB1 expression in NRCMs and measured changes in cell surface area following SZC-6 therapy. LKB1 knockdown reversed the effect of SZC-6 on cell surface size (Supplementary Fig. S7). In cardiac tissues, LKB1 mediated AMPK phosphorylation. When intracellular ATP concentrations dropped, AMPK was activated as a major metabolic sensor. The next question we sought to address was whether AMPK was involved in protecting against mitochondrial dysfunction by SZC-6. The results demonstrated that in the heart tissues of mice treated with SZC-6, phosphorylation of AMPK (Thr172) and the downstream substrate acetyl coenzyme A carboxylase (ACC) (Ser79) were dramatically increased, but not in SIRT3-KO mice (Fig. 8d). In addition, LKB1 knockdown with siRNA blocked SZC-6-induced phosphorylation of ACC and AMPK in NRCMs (Fig. 8e–h). Therefore, SZC-6 could activate the LKB1/AMPK pathway in vitro and in vivo. AMPK regulated intracellular energy levels and mitochondrial organization after activation. Mito-Tracker Red stain revealed mitochondrial fission and demonstrated that SZC-6 decreased ISO-induced mitochondrial fission in NRCMs, and knockdown of AMPK and LKB1 blocked the effect of SZC-6. Phosphorylation of Drp1 at Ser 616 is a hallmark of Drp1 activation [45]. Increased depolarization of mitochondria enhanced cytosolic p-Drp1 recruitment, which facilitated mitochondrial fission. We observed a decrease in Drp1-Ser616 phosphorylation in mitochondria by SZC-6 compared to the ISO group. By contrast, siRNA targeting AMPK and AMPK inhibitor (Compound C, CC) attenuated

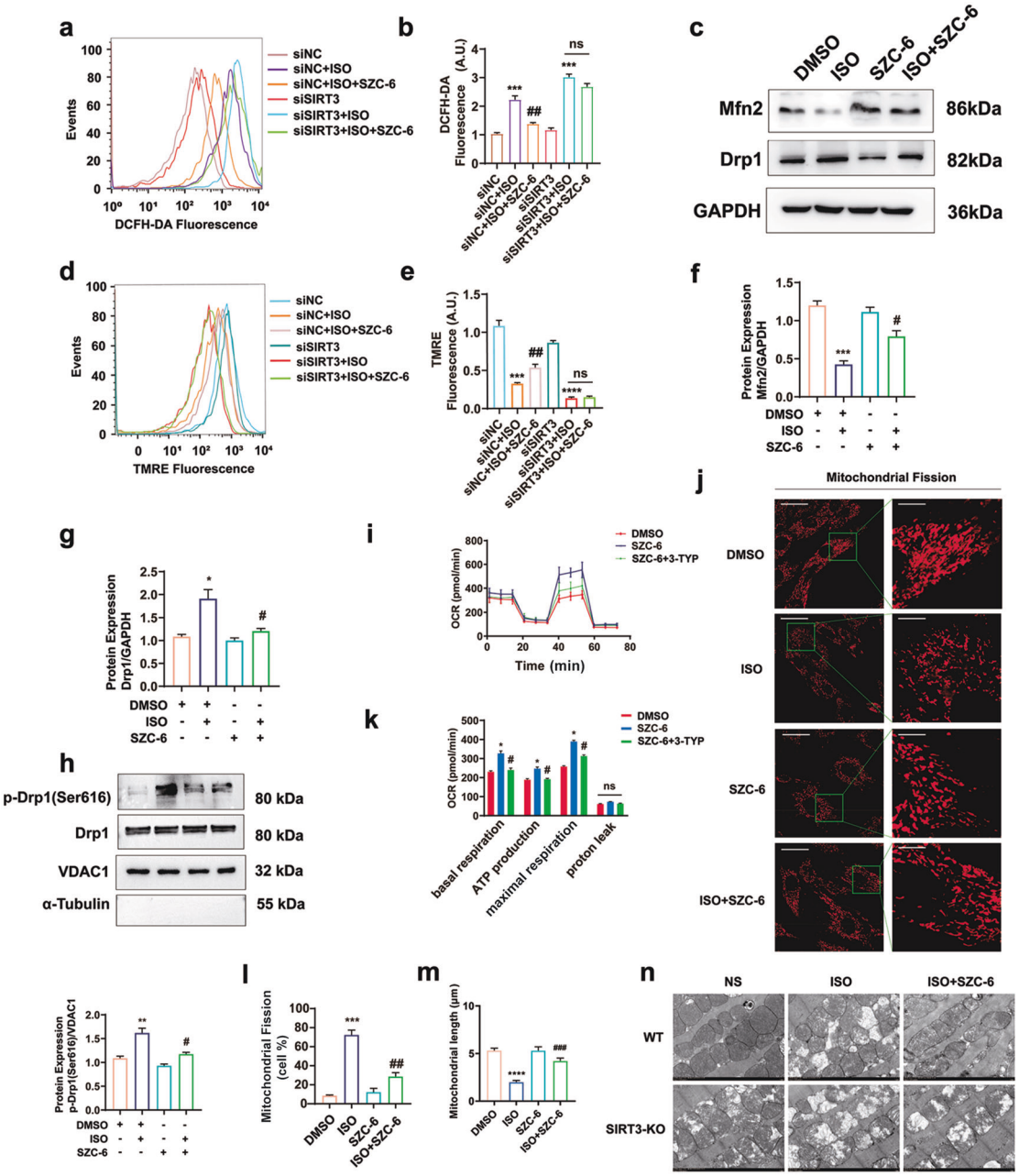

Fig. 7 SZC-6 improves mitochondrial function via SIRT3. a, **b** NRCMs were transfected with si-SIRT3 or siNC, followed by incubation with ISO (10 μM for 24 h) in the presence or absence of 10 μM SZC-6. Cells were stained with DCFH-DA. ROS levels were measured by FACS analysis. The data are presented as the mean ± SEM. $^{***}P < 0.001$ *vs*. the siNC group or the siSIRT3 group; $^{\#\#}P < 0.01$ *vs*. the siNC+ISO group; $n = 4$. **c**, **f**, **g** Immunoprecipitation analysis showed the protein level of Mfn2 and Drp1. Data are presented as means ± SEM, $^{*}P < 0.05$, $^{***}P < 0.001$ *vs*. the DMSO group; $^{\#}P < 0.05$ *vs*. the ISO group; $n = 4$. **d**, **e** NRCMs were stained with TMRE and subjected to FACS analysis. Data are presented as means ± SEM $^{***}P < 0.001$, $^{****}P < 0.0001$ *vs*. the siNC group; $^{\#\#}P < 0.05$ *vs*· the ISO group; $n = 4$. **h** The expression of p-Drp1(Ser 616) and Drp1 in the mitochondrial fractions of H9c2 was determined. The data are presented as the mean ± SEM. $^{**}P < 0.01$ *vs*. the DMSO group; $^{\#}P < 0.05$ *vs*. the ISO group; $n = 4$. **i**, **k** H9c2 cells were pretreated with 3-TYP or negative control for 12 h and then incubated with 10 μM SZC-6 or DMSO. The oxygen consumption rate (OCR) and respiration parameters, including basal respiration, ATP production, maximal respiration and H^+ leak, were detected by using a Seahorse XF96 Analyzer. The data are presented as the mean ± SEM. $^{*}P < 0.05$ *vs*· the DMSO group; $^{\#}P < 0.05$ *vs*. the SZC-6 group; $n = 3$. **j**, **l** NRCMs were incubated with 10 μM SZC-6 or DMSO and treated with ISO for 24 h. Mitochondrial fission was detected by MitoTracker Red with confocal microscopy. Left, scale bar, 20 μm; right, magnified images, bar, 5 μm. The results were expressed as the mean ± SEM. $^{***}P < 0.001$ *vs*. the DMSO group; $^{\#\#}P < 0.001$ *vs*. the ISO group; $n = 3$. **m** Quantification of mitochondrial length is shown. More than 30 cells were assessed. $^{****}P < 0.0001$ *vs*. the DMSO group. $^{\#\#\#}P < 0.001$ *vs*. the ISO group. **n** The mitochondrial ultrastructure of cardiac tissues was detected by TEM. Representative images of four independent samples are shown (scale bar = 1 μm).

the above results (Fig. 8j and Supplementary Fig. S8). Knockdown of either LKB1 or AMPK reversed the inhibitory effect of SZC-6 on mitochondrial hyperfission (Fig. 8k, l, m). To clarify whether AMPK and LKB1 were involved in the protective effect of SZC-6 on mitochondrial antioxidant function, we utilized the mitochondrial-specific ROS indicator MitoSOX Red to detect superoxide in the mitochondria of live cells. The results revealed that MitoSOX fluorescence was decreased in SZC-6 pre-treated cells compared with the ISO group, while siRNA targeting AMPK and LKB1 demolished this effect (Fig. 8i). These results implied that LKB1/AMPK participated in the protective effect of SZC-6 on mitochondria. The activation of SIRT3 by SZC-6 had an antioxidant, mitochondrial-protective, and cytoprotective effect in the current study, at least in part due to AMPK activation mediated by LKB1.

DISCUSSION

In this study, a specific SIRT3 activator was discovered that reduced heart hypertrophic responses in mice. Through in vitro and in vivo analyses, SZC-6 bound to SIRT3 and directly activated its deacetylation. Subsequently, increased phosphorylation of LKB1 might regulate heart function by maintaining cardiac LKB1-AMPK signaling orchestrating mitochondrial fission and oxidative stress. Furthermore, SZC-6 therapy reduced the generation of cardiac fibrosis by inhibiting fibroblast growth and transformation into myofibroblasts, according to our findings.

In response to mechanical and/or pathological stress, adult mammalian hearts commonly undergo mal-remodeling, which is known as pathological hypertrophy [46]. Cardiovascular disease was caused by persistent heart enlargement, which led to a variety of clinical abnormalities [47]. Understanding the molecular basis of cardiac hypertrophy has progressed dramatically in recent years. Previous studies have revealed that over 200 cardiac mitochondrial proteins were acetylated without hypertrophic stimuli, and their acetylation status would change in response to hypertrophic stimuli [48]. Targeting deacetylase that maintains the balance of acetylation status in heart should provides an approach for the specific inhibition of cardiac myocyte hypertrophy and for the development of novel strategies to prevent and treat heart failure.

Sirtuins have been implicated in pathological cardiac hypertrophy in previous research from our lab and others [3, 49–51]. SIRT4 prevented the binding of MnSOD to SIRT3, another mitochondrial sirtuin, and increased MnSOD acetylation levels to limit its activity, resulting in increased ROS generation under hypertrophic stimulation [52]. In addition, SIRT3 has been shown to deacetylate and activate mitochondrial enzymes involved in fatty acid oxidation and amino acid metabolism. Age-related cardiac hypertrophy, the electron transport chain, and antioxidant defences were all suppressed by SIRT3-mediated deacetylation of cyclophilin D [33]. Therefore, according to these researches, SIRT3 might be a promising therapeutic target for heart hypertrophy.

Several SIRT3 agonists has been reported previously, most of which were derived from natural products. Polydatin, a polyphenolic substance derived from Polygonum, could regulate mitochondrial autophagy to rescue cardiomyocytes by elevating SIRT3 expression [53]. A well-established SIRT1 activator, Resveratrol, was reported to increase SIRT3 expression and alleviate acute kidney injury [54]. Furthermore, HKL was famous for its ability to inhibit and reverse heart hypertrophy in mice via activating SIRT3, as indicated by decreased acetylation levels of MnSOD and OSCP [24]. However, there was a lack of sufficient experimental data to evaluate the biological activity of these compounds. Among these SIRT3 agonists, 7-hydroxy-3-(4′-methoxyphenyl) coumarin (C12) was the only one identified based on the crystal structure of an acetylated substrate of SIRT3. The results showed that MnSOD deacetylation and activation were enhanced by C12. It was worth mentioning that C12 provided a theoretical foundation for designing the SIRT3 activator [55]. In our studies, the K_d value of SZC-6 combined with SIRT3 was 15 μM based on the SPR assay and the 50% activation of acetylated substrates was under 23.2 μM of SZC-6, while the K_d value of C12 was 24.3 μM and 50% activation concentration was 71.8 μM. These results suggested that SZC-6 had high activity, comparable to existing SIRT3 agonists. Furthermore, 14-day SZC-6 treatment of 60 $mg{\cdot}kg^{-1}{\cdot}d^{-1}$ was sufficient to relieve ventricular hypertrophy in mice without causing severe damage. Even if in the ISO-induced heart failure model, SZC-6-mediated activation of SIRT3 rescue the cardiac function in terms of EF, FS, LVPW, and LVIDs (Supplementary Fig. S9). Above all, SZC-6 was a new promising SIRT3 agonist candidate for the treatment of cardiac dysfunction.

There are other flavonoid compounds reported as SIRT activators. For instance, Cyanidin is a flavonoid compound that was reported to activate SIRT6 with high potency and efficacy [56]. Both SZC-6 and quercetin have the catechol moiety that is buried in a protein pocket and their 4′-hydroxyl groups form a hydrogen bond to the backbone oxygen and the 4′-hydroxyl form water-mediated interactions with SIRT. These structural features allow SZC-6 and quercetin to donate hydrogen to scavenge free radicals and increase the stability of flavonoid radicals. Moreover, the substitution with Br allowed slight rotation of the catechol moiety of SZC-6, and more drastically in a tilted position of the chroman, orienting them toward the N-terminus. It thus appears that the buried catechol group of SZC-6 functions as an anchor in SIRT3 binding, while the chromen-2-one provides smaller and non-specific binding contributions. This might be particularly amenable for modifications to increase compound affinity with SIRT family members in the future.

Considering that SZC-6 contains a typical coumarin core, there are potential off-target effects of SZC-6 in its cardioprotection. Several coumarin derivatives were reported as selective monoamine oxidase B (MAO-B) inhibitors which prevent LV dilation and functional decompensation in hearts subjected to pressure overload [57]. As inhibiting MAO-B can prevent mitochondrial dysfunction, MAO-B inhibition may also be involved in SZC-6-mediated mitochondrial protection. However, positive allosteric modulators like SZC-6 only work when the natural ligand is present in vivo, reducing potential side effects of constitutively active agonists [58]. This is the obvious advantage of SZC-6 over other traditional SIRT3 agonists.

SIRT3 could bind to LKB1 and deacetylate. Supportively, according to our findings, the ISO-induced reduction in LKB1 phosphorylation of cardiomyocytes was evenly correlated with the increase in LKB1 acetylation. In neonatal rats' primary cardiac cells, the connections between SIRT3 and LKB1 were detected. In mice, knocking down LKB1 in cardiomyocytes could result in cardiac hypertrophy via the inhibition of AMPK signaling and the activation of mTOR signaling. Supportively, we observed SIRT3 deficiency reduced LKB1 phosphorylation in ISO-induced hypertrophic hearts, whereas SZC-6 elevated LKB1 phosphorylation in dilated hearts of wild-type mice. Upregulation of AMPK signaling, a well-known regulator of cellular energy balance, has been demonstrated to regulate multiple important signaling pathways involved in cardiomyocyte growth control, which was also found in SZC-6 supplemented cells. Therefore, SZC-6 played a critical role in cardiac hypertrophy regulation via modulating LKB1/AMPK signaling.

So far, mitochondrial dysfunction has been proven to be involved in the start and development of hypertrophy [59]. Ninety percent of the ATP required for myocardial contractility originated from myocardial mitochondrial metabolism [60]. In aging rat hearts, experimental studies have indicated an elevation in mitochondrial ROS production as well as a more disordered and accompanying decline in ATP levels, mitochondrial membrane depolarization, and changes in mitochondrial dynamics [61, 62]. SIRT3 was involved in a variety of mitochondrial processes, including ATP production and energy metabolism, anti-oxidant

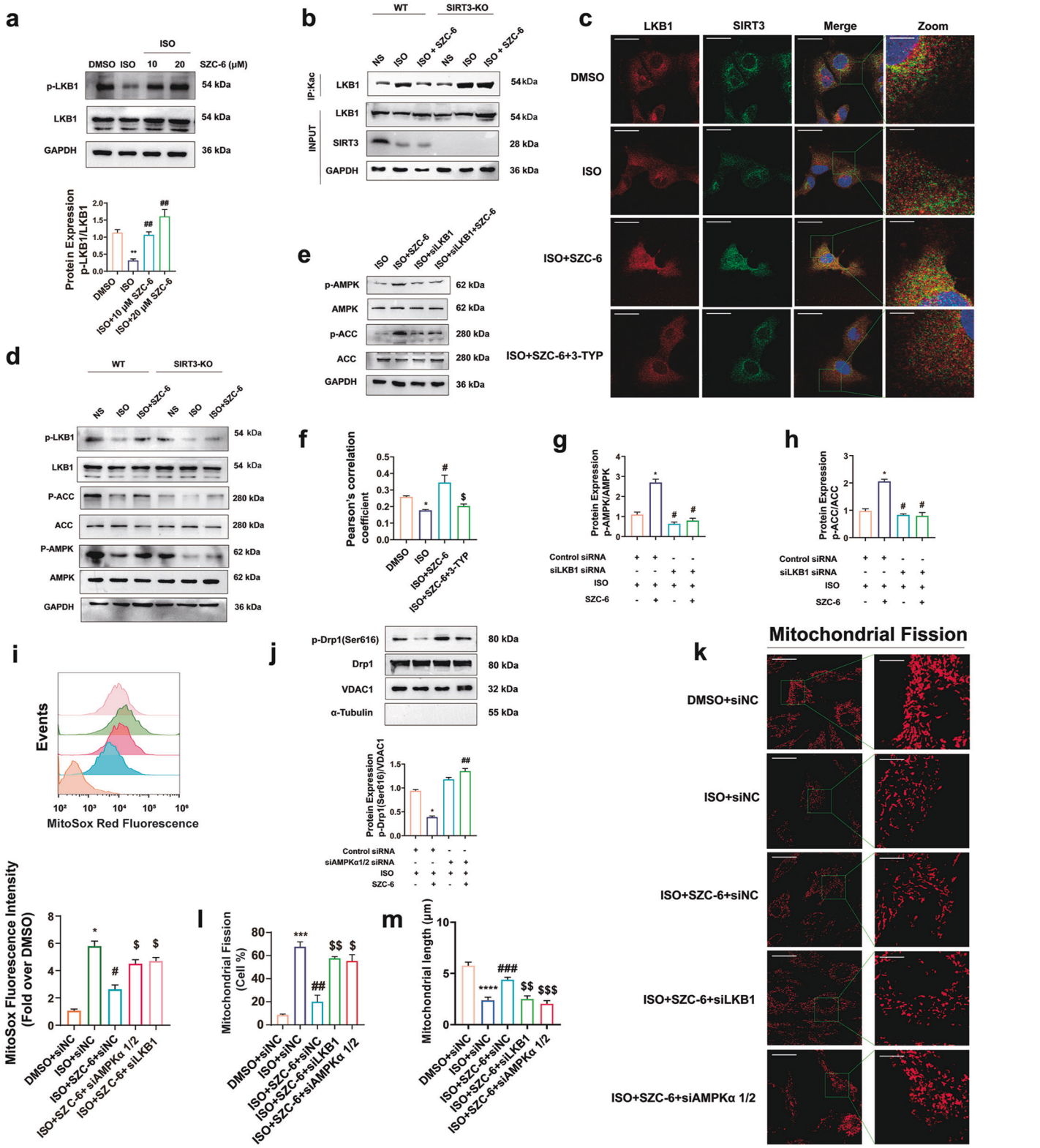

defense, cell death, and proliferation. SIRT3 could deacetylate transcriptional factors and interact with many signaling pathways to regulate mitochondrial quality control systems and collaboratively alter mitochondrial activities. SZC-6 activated SIRT3 in our investigation, and this was accompanied by an elevation in mitochondrial membrane potential, basal respiration, ATP generation, and reduced mitochondiral ROS. However, SIRT3 inhibition eliminated SZC-6's cardioprotective impact. Overall, these findings suggested that SZC-6-induced SIRT3 activation might help safeguard mitochondrial function.

Changes in energy metabolism affected mitochondrial fission and fusion rates. In mice, increased mitochondrial fission might

Fig. 8 SZC-6 protects mitochondrial integrity by activating SIRT3/LKB1/AMPK signaling. a NRCMs were incubated with SZC-6 or DMSO, followed by incubation with ISO (10 μM for 24 h). The protein expression of p-LKB1 and total LKB1 was measured by Western blotting. $^{**}P < 0.01$ *vs*. the DMSO group; $^{\#\#}P < 0.05$ *vs*. the ISO group; $n = 4$. **b** Immunoprecipitation analysis showed the acetylation levels of LKB1 in cardiac tissue after treatment with SZC-6. Representative images are shown. **c**, **f** NRCMs obtained from WT and SIRT3-KO mice were pretreated with 3-TYP or negative control for 12 h and then incubated with ISO in the presence or absence of SZC-6 for 24 h. Cells were immunostained for SIRT3 and LKB1. Left, scale bar, 20 μm; right, magnified images, bar, 5 μm. The extent of colocalization of SIRT3 and LKB1 was determined by calculating the Pearson correlation coefficient from 20 independent fields of cells in 3 different experiments. $^{*}P < 0.05$ *vs*. the DMSO group; $^{\#}P < 0.05$ *vs*. the ISO group; $^{\$}P < 0.05$ *vs*. the ISO + SZC-6 group; $n = 4$. **d** The phosphorylation levels of LKB1, AMPK and ACC in cardiac tissues were measured by Western blot analysis. **e**, **g**, **h** The phosphorylation levels of LKB1, AMPK and ACC. **i** NRCMs were stained with MitoSox Red and subjected to FACS analysis. Data are presented as means ± SEM, $^{*}P < 0.05$ *vs*. the DMSO group; $^{\#}P < 0.05$ *vs*. the ISO group; $^{\$}P < 0.05$ *vs*. the ISO+SZC-6+siNC. $n = 4$. **j** The expression of p-Drp1(Ser 616) and Drp1 in the mitochondrial fractions of H9c2 was determined. The data are presented as the mean ± SEM. $^{*}P < 0.05$ *vs*. the ISO + Control siRNA group; $^{\#\#}P < 0.01$ *vs*. the ISO + Control siRNA+SZC-6 group; $n = 4$. **k**, **l**, **m** NRCMs were transfected for 24 h, followed by incubation with ISO (10 μM for 24 h) in the presence or absence of SZC-6. Mitochondrial fission was detected by MitoTracker Red with confocal microscopy. Left, scale bar, 20 μm; right, magnified images, bar, 5 μm. Quantification of mitochondrial length is shown, more than 30 cells were assessed. The results were expressed as the mean ± SEM. $^{***}P < 0.001$, $^{****}P < 0.0001$ *vs*. the DMSO + siNC group; $^{\#\#}P < 0.01$, $^{\#\#\#}P < 0.001$ *vs*. the ISO + siNC group; $^{\$}P < 0.05$, $^{\$\$}P < 0.01$, $^{\$\$\$}P < 0.001$ *vs*. the ISO + SZC-6+siNC group; $n = 3$

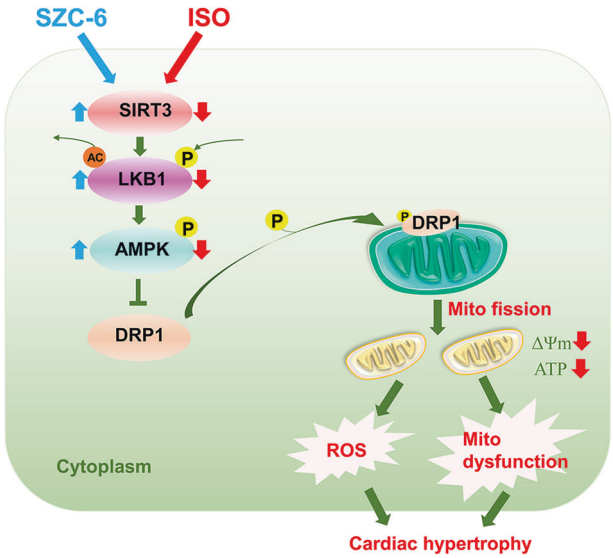

Fig. 9 Schematic of the proposed role of SZC-6 in ISO-induced cardiac hypertrophy. Schematic of the proposed role of SZC-6 in ISO-induced cardiac hypertrophy. When cells are exposed to ISO stimulation, the expression of SIRT3 is significantly downregulated. SZC-6 directly activated SIRT3 and decreased the acetylation level of LKB1 by increasing the interaction between LKB1 and SIRT3, which was accompanied by an increase in the phosphorylation level of LKB1 and the activation of AMPK. The upregulation of AMPK activity resulted in a decrease in the phosphorylation level of Drp1 at the Ser616. The reduction of Drp1 recruitment to mitochondria resulted in the inhibition of ISO stimulation-induced mitochondrial division and serves the protective effect of mitochondria. Collectively, these effects attenuate the development of cardiac hypertrophy

hasten mitochondrial dysfunction and heart failure. Abnormal morphologic alterations had an impact on the production of ATP and probably exacerbated the problem by releasing even more ROS [59, 63]. AMPK could increase mitochondrial fission directly in response to severe stress by phosphorylating Ser616 and dephosphorylating Ser637 of Drp1 [64]. In our studies, we found that AMPK was associated with ISO-induced mitochondrial fragmentation. SZC-6 inhibited mitochondrial fission by reducing mitochondrial ROS production and phosphorylation of Drp1 at Ser 616. The effect of SZC-6 in controlling Drp1 phosphorylation was inhibited when AMPK was knocked down with specific siRNA, demonstrating that SZC-6 preserved mitochondrial integrity against ROS stress in an AMPK-dependent way.

In this work, the anti-cardiac hypertrophy action of SZC-6 was successfully demonstrated, and SZC-6 was identified as a high-potency SIRT3 activator. We firstly found that SZC-6 significantly reduced the acetylation level of cardiac mitochondrial proteins. The results of this work proved that SZC-6 inhibited the progression of heart hypertrophy both in vitro and in vivo. Importantly, SZC-6 improved mitochondrial function as determined by cellular respiration, mitochondrial membrane potential and ATP analysis. In addition, SZC-6 inhibited the ISO stimulation-induced imbalance of mitochondrial dynamics by activating the LKB1/AMPK/Drp1 pathway. Based on our results supplied here and previously available data, we proposed a hypothesis that explained the likely mechanism behind SIRT3 activation by SZC-6 (Fig. 9). Briefly, SZC-6 maintained mitochondrial dynamic homeostasis through the LKB1/AMPK/Drp1 pathway, accompanied by reducing oxidative stress and increasing energy production. SZC-6, a novel SIRT3 activator, was expected to facilitate the creation of new treatments for cardiac hypertrophy and other SIRT3-related diseases.

ACKNOWLEDGEMENTS

This work was supported by the National Natural Science Foundation of China (U21A20419, 82173808, 82150204, 81872860, 82104157), Natural Science Foundation of Guangdong Province (2021B1515020100, 2022A1515012322, 2016A030311033), the Basic and Applied Basic Research Foundation of Guangdong Province (2020A1515410003), National Engineering and Technology Research Center for New drug Druggability Evaluation (Seed Program of Guangdong Province, 2017B090903004), Guangzhou Basic and Applied Basic Research Project (202102020173) and Guangdong Provincial Key Laboratory of Construction Foundation (2017B030314030), the Fundamental Research Funds for the Central Universities, Sun Yat-sen University (22qntd4510).

AUTHOR CONTRIBUTIONS

PQL, YZ and XLZ were responsible for the experimental design and supervision of this project. ZYL performed most of the experiments and was the main writer of the manuscript. ZYL and PXW contributed to animal experiments. GQL contributed to the synthesis of compounds. JL contributed to the data analysis and manuscript writing. All authors made important suggestions regarding the manuscript.

ADDITIONAL INFORMATION

Supplementary information The online version contains supplementary material available at https://doi.org/10.1038/s41401-022-00966-8.

Competing interests: The authors declare no competing interests.

REFERENCES

1. Lu JQ, Zhang H, Chen X, Zou Y, Li JS, Wang L, et al. A small molecule activator of SIRT3 promotes deacetylation and activation of manganese superoxide dismutase. Free Radic Biol Med. 2017;112:287–97.

2. Lin ZQ, Murtaza I, Wang K, Jiao JQ, Gao J, Li PF. MiR-23a functions downstream of NFATc3 to regulate cardiac hypertrophy. Proc Natl Acad Sci USA. 2009;106:12103–8.
3. Ding YQ, Zhang YH, Lu J, Li B, Yu WJ, Yue ZB, et al. MicroRNA-214 contributes to Ang II-induced cardiac hypertrophy by targeting SIRT3 to provoke mitochondrial malfunction. Acta Pharmacol Sin. 2021;42:1422–36.
4. Kim TS, Jin YB, Kim YS, Kim S, Kim JK, Lee HM, et al. SIRT3 promotes antimycobacterial defenses by coordinating mitochondrial and autophagic functions. Autophagy. 2019;15:1356–75.
5. Hallows WC, Yu W, Smith BC, Devries MK, Ellinger JJ, Someya S, et al. Sirt3 promotes the urea cycle and fatty acid oxidation during dietary restriction. Mol Cell. 2011;41:139–49.
6. Gu DC, Chen CY, Zhao ML, Zhao LM, Duan XW, Duan J, et al. Identification of HDA15-PIF1 as a key repression module directing the transcriptional network of seed germination in the dark. Nucleic Acids Res. 2017;45:7137–50.
7. Jiang WQ, Wang SW, Xiao MT, Lin Y, Zhou LS, Lei QY, et al. Acetylation regulates gluconeogenesis by promoting PEPCK1 degradation via recruiting the UBR5 ubiquitin ligase. Mol Cell. 2011;43:33–44.
8. Wellman AS, Metukuri MR, Kazgan N, Xu XJ, Xu Q, Ren NSX, et al. Intestinal epithelial sirtuin 1 regulates intestinal inflammation during aging in mice by altering the intestinal microbiota. Gastroenterology. 2017;153:772–86.
9. Jeong SM, Xiao CY, Finley LWS, Lahusen T, Souza AL, Pierce K, et al. SIRT4 has tumor-suppressive activity and regulates the cellular metabolic response to DNA damage by inhibiting mitochondrial glutamine metabolism. Cancer Cell. 2013;23:450–63.
10. Rardin MJ, He WJ, Nishida Y, Newman JC, Carrico C, Danielson SR, et al. SIRT5 regulates the mitochondrial lysine succinylome and metabolic networks. Cell Metab. 2013;18:920–33.
11. Zhang XK, Ji RP, Liao XH, Castillero E, Kennel PJ, Brunjes DL, et al. MicroRNA-195 regulates metabolism in failing myocardium via alterations in sirtuin 3 expression and mitochondrial protein acetylation. Circulation. 2018;137:2052–67.
12. Zhang J, Xiang H, Liu J, Chen Y, He RR, Liu B. Mitochondrial sirtuin 3: new emerging biological function and therapeutic target. Theranostics. 2020;10:8315–42.
13. Wei T, Gao J, Huang C, Song B, Sun M, Shen WL. SIRT3 (sirtuin-3) prevents Ang II (angiotensin II)-induced macrophage metabolic switch improving perivascular adipose tissue function. Arterioscler Thromb Vasc Biol. 2021;41:714–30.
14. Sun W, Liu CX, Chen QH, Liu N, Yan YY, Liu B. SIRT3: a new rregulator of cardiovascular diseases. Oxid Med Cell Longev. 2018;2018:1–11.
15. Liu LJ, Nam M, Fan W, Akie TE, Hoaglin DC, Gao GP, et al. Nutrient sensing by the mitochondrial transcription machinery dictates oxidative phosphorylation. J Clin Invest. 2014;124:768–84.
16. Zhang X, Ren X, Zhang Q, Li Z, Ma S, Bao J, et al. PGC-1α/ERRα-Sirt3 pathway regulates DAergic neuronal death by directly deacetylating SOD2 and ATP Synthase β. Antioxid Redox Signal. 2016;24:312–28.
17. Vassilopoulos A, Pennington J, Andresson T, Rees D, Bosley A, Fearnley I, et al. SIRT3 deacetylates ATP synthase F1 complex proteins in response to nutrient- and exercise-induced stress. Antioxid Redox Signal. 2014;21:551–64.
18. Hirschey MD, Shimazu T, Jing E, Grueter CA, Collins AM, Aouizerat B, et al. SIRT3 deficiency and mitochondrial protein hyperacetylation accelerate the development of the metabolic syndrome. Mol Cell. 2011;44:177–90.
19. Jing EX, Emanuelli B, Boucher J, Carmona J, Kim B, Kahn CR. Sirt3, a novel nutrient sensor and regulator of insulin signaling in diabetes and insulin resistance. Diabetes. 2008;57:A44–A.
20. Tomczyk M, Cheung K, Xiang B, Tamanna N, Fonseca Teixeira A, Agarwal P, et al. Mitochondrial sirtuin-3 (SIRT3) prevents doxorubicin-induced dilated cardiomyopathy by modulating protein acetylation and oxidative stress. J Biol Chem. 2022;15:e008547.
21. Morishima C, Shuhart MC, Wang CC, Paschal DM, Apodaca MC, Liu YZ, et al. Silymarin inhibits in vitro T-cell proliferation and cytokine production in hepatitis c virus infection. Gastroenterology. 2010;138:671–U332.
22. Li Y, Ye ZC, Lai WY, Rao JL, Huang WB, Zhang XH, et al. Activation of sirtuin 3 by silybin attenuates mitochondrial dysfunction in cisplatin-induced acute kidney injury. Front Pharmacol. 2017;8:178.
23. Pillai VB, Kanwal A, Fang YH, Sharp WW, Samant S, Arbiser J, et al. Honokiol, an activator of Sirtuin-3 (SIRT3) preserves mitochondria and protects the heart from doxorubicin-induced cardiomyopathy in mice. Oncotarget. 2017;8:34082–98.
24. Pillai VB, Samant S, Sundaresan NR, Raghuraman H, Kim G, Bonner MY, et al. Honokiol blocks and reverses cardiac hypertrophy in mice by activating mitochondrial Sirt3. Nat Commun. 2015;6:6656.
25. Wang M, Li Y, Ni CW, Song GJ. Honokiol attenuates oligomeric amyloid beta(1-42)-induced alzheimer's disease in mice through attenuating mitochondrial apoptosis and inhibiting the nuclear factor kappa-B signaling pathway. Cell Physiol Biochem. 2017;43:69–81.
26. Li J, Huang J, Lu J, Guo Z, Li Z, Gao H, et al. Sirtuin 1 represses PKC-ζ activity through regulating interplay of acetylation and phosphorylation in cardiac hypertrophy. Br J Pharmacol. 2019;176:416–35.
27. Wang PX, Wang LP, Lu J, Hu YH, Wang QQ, Li ZZ, et al. SESN2 protects against doxorubicin-induced cardiomyopathy via rescuing mitophagy and improving mitochondrial function. J Mol Cell Cardiol. 2019;133:125–37.
28. Fu J, Gao J, Pi R, Liu P. An optimized protocol for culture of cardiomyocyte from neonatal rat. Cytotechnology. 2005;49:109–16.
29. Song M, Sandoval TA, Chae CS, Chopra S, Tan C, Rutkowski MR, et al. IRE1α-XBP1 controls T cell function in ovarian cancer by regulating mitochondrial activity. Nature. 2018;562:423–8.
30. Li X, Dai F, Wang H, Wei G, Jiang Q, Yin P, et al. PCSK9 participates in oxidized-low density lipoprotein-induced myocardial injury through mitochondrial oxidative stress and Drp1-mediated mitochondrial fission. Clin Transl Med. 2022;12:e729.
31. Huang ZM, Zhao JX, Deng W, Chen YY, Shang JL, Song K, et al. Identification of a cellularly active SIRT6 allosteric activator. Nat Chem Biol. 2018;14:1118–26.
32. Yoshino J, Mills KF, Yoon MJ, Imai SI. Nicotinamide mononucleotide, a key NAD^+ intermediate, treats the pathophysiology of diet- and age-Induced diabetes in mice. Cell Metab. 2011;14:528–36.
33. Cheng AW, Yang Y, Zhou Y, Maharana C, Lu DY, Peng W, et al. Mitochondrial SIRT3 mediates adaptive responses of neurons to exercise and metabolic and excitatory challenges. Cell Metab. 2016;23:128–42.
34. Hsu CP, Oka S, Shao D, Hariharan N, Sadoshima J. Nicotinamide phosphoribosyltransferase regulates cell survival through NAD^+ synthesis in cardiac myocytes. Circ Res. 2009;105:481–U193.
35. Ma LL, Kong FJ, Ma YJ, Guo JJ, Wang SJ, Dong Z, et al. Hypertrophic preconditioning attenuates post-myocardial infarction injury through deacetylation of isocitrate dehydrogenase 2. Acta Pharmacol Sin. 2021;42:2004–15.
36. Sundaresan NR, Gupta M, Kim G, Rajamohan SB, Isbatan A, Gupta MP. Sirt3 blocks the cardiac hypertrophic response by augmenting Foxo3a-dependent antioxidant defense mechanisms in mice. J Clin Invest. 2009;119:2758–71.
37. Osio A, Tan L, Chen SN, Lombardi R, Nagueh SF, Shete S, et al. Myozenin 2 is a novel gene for human hypertrophic cardiomyopathy. Circ Res. 2007;100:766–8.
38. Kondo K, Bhushan S, King AL, Prabhu SD, Hamid T, Koenig S, et al. H_2S protects against pressure overload-induced heart failure via upregulation of endothelial nitric oxide synthase. Circulation. 2013;127:1116–27.
39. Hu TP, Xu FP, Li YJ, Luo JD. Simvastatin inhibits leptin-induced hypertrophy in cultured neonatal rat cardiomyocytes. Acta Pharmacol Sin. 2006;27:419–22.
40. Xu HX, Cui SM, Zhang YM, Ren J. Mitochondrial Ca^{2+} regulation in the etiology of heart failure: physiological and pathophysiological implications. Acta Pharmacol Sin. 2020;41:1301–9.
41. Jo DS, Park SJ, Kim AK, Park NY, Kim JB, Bae JE, et al. Loss of HSPA9 induces peroxisomal degradation by increasing pexophagy. Autophagy. 2020;16:1989–2003.
42. Jin JY, Wei XX, Zhi XL, Wang XH, Meng D. Drp1-dependent mitochondrial fission in cardiovascular disease. Acta Pharmacol Sin. 2021;42:655–64.
43. Wang LT, He PC, Li AQ, Cao KX, Yan JW, Guo S, et al. Caffeine promotes angiogenesis through modulating endothelial mitochondrial dynamics. Acta Pharmacol Sin. 2021;42:2033–45.
44. Qi DK, Atsina K, Qu LT, Hu XY, Wu XH, Xu B, et al. The vestigial enzyme D-dopachrome tautomerase protects the heart against ischemic injury. J Clin Invest. 2014;124:3540–50.
45. Zhang T, Liu JX, Shen SN, Tong Q, Ma XJ, Lin LG. SIRT3 promotes lipophagy and chaperon-mediated autophagy to protect hepatocytes against lipotoxicity. Cell Death Differ. 2020;27:329–44.
46. Seok HY, Chen JH, Kataoka M, Huang ZP, Ding J, Yan JL, et al. Loss of MicroRNA-155 Protects the heart from pathological cardiac hypertrophy. Circ Res. 2014;114:1585–95.
47. Jensen MK, Bartz TM, Mukamal KJ, Djousse L, Kizer JR, Tracy RP, et al. Fetuin-A, type 2 diabetes, and risk of cardiovascular disease in older aadults the cardiovascular health study. Diabetes Care. 2013;36:1222–8.
48. Nguyen TTM, Wong R, Menazza S, Sun JH, Chen Y, Wang GH, et al. Cyclophilin d modulates mitochondrial acetylome. Circ Res. 2013;113:1308–19.
49. Yue ZB, Ma YZ, You J, Li ZM, Ding YQ, He P, et al. NMNAT3 is involved in the protective effect of SIRT3 in Ang II-induced cardiac hypertrophy. Exp Cell Res. 2016;347:261–73.
50. Li ZZ, Zhang XY, Guo Z, Zhong Y, Wang PX, Li JY, et al. SIRT6 suppresses NFATc4 expression and activation in cardiomyocyte hypertrophy. Front Pharmacol. 2019;9:1519.
51. Shen PY, Feng XJ, Zhang XY, Huang XY, Liu SL, Lu X, et al. SIRT6 suppresses phenylephrine-induced cardiomyocyte hypertrophy though inhibiting p300. J Pharm Sci. 2016;132:31–40.
52. Tang XQ, Chen XF, Wang NY, Wang XM, Liang ST, Zheng W, et al. SIRT2 acts as a cardioprotective deacetylase in pathological cardiac hypertrophy. Circulation. 2017;136:2051–67.
53. Zhang MM, Zhao ZJ, Shen M, Zhang YM, Duan JH, Guo YJ, et al. Polydatin protects cardiomyocytes against myocardial infarction injury by activating Sirt3. Biochim Biophys Acta Mol Basis Dis. 2017;1863:1962–72.

54. Srivastava SP, Li JP, Kitada M, Fujita H, Yamada Y, Goodwin JE, et al. SIRT3 deficiency leads to induction of abnormal glycolysis in diabetic kidney with fibrosis. Cell Death Dis. 2018;9:997.
55. Lu J, Zhang H, Chen X, Zou Y, Li J, Wang L, et al. A small molecule activator of SIRT3 promotes deacetylation and activation of manganese superoxide dismutase. Free Radic Biol Med. 2017;112:287–97.
56. Akter R, Afrose A, Rahman MR, Chowdhury R, Nirzhor SSR, Khan RI, et al. A comprehensive analysis into the therapeutic application of natural products as SIRT6 modulators in alzheimer's disease, aging, ccancer, inflammation, and diabetes. Int J Mol Sci. 2021;22:4180.
57. Heger J, Hirschhäuser C, Bornbaum J, Sydykov A, Dempfle A, Schneider A, et al. Cardiomyocytes-specific deletion of monoamine oxidase B reduces irreversible myocardial ischemia/reperfusion injury. Free Radic Biol Med. 2021;165:14–23.
58. Zhang F, Klebansky B, Fine R, Xu H, Pronin A, Liu H, et al. Molecular mechanism for the umami taste synergism. Proc Natl Acad Sci USA. 2008;105:20930–4.
59. Karamanlidis G, Nascimben L, Couper GS, Shekar PS, del Monte F, Tian R. Defective DNA replication impairs mitochondrial biogenesis in human failing hearts. Circ Res. 2010;106:1541–8.
60. Doenst T, Nguyen TD, Abel ED. Cardiac metabolism in heart failure implications beyond ATP production. Circ Res. 2013;113:709–24.
61. Karamanlidis G, Lee CF, Garcia-Menendez L, Kolwicz SC, Suthammarak W, Gong GH, et al. Mitochondrial complex I deficiency increases protein acetylation and accelerates heart Failure. Cell Metab. 2013;18:239–50.
62. Zhu X, Shen W, Yao K, Wang H, Liu B, Li T, et al. Fine-tuning of PGC1α expression regulates cardiac function and longevity. Circ Res. 2019;125:707–19.
63. Wu S, Lu Q, Wang Q, Ding Y, Ma Z, Mao X, et al. Binding of FUN14 domain containing 1 with inositol 1,4,5-trisphosphate receptor in mitochondria-associated endoplasmic reticulum membranes maintains mitochondrial dynamics and function in hearts in vivo. Circulation. 2017;136:2248–66.
64. Zhou H, Hu N, Cao F, Chen YD, Ren J. Melatonin protects cardiac microvasculature against ischemia/reperfusion injury via suppression of mitochondrial fission/VDAC1/HK2/mPTP/Mitophagy axis. J Pineal Res. 2017;63:e12413.